Residence and redistribution of REE, Y, Zr, Th and U during granulite-facies metamorphism: behaviour of accessory and major phases in peraluminous granulites of central Spain

C. Villaseca[a,*], C. Martín Romera[a], J. De la Rosa[b], L. Barbero[c]

[a] *Departamento Petrología y Geoquímica, Facultad Ciencias Geológicas, UCM, Universidad Complutense, 28040 Madrid, Spain*
[b] *Departamento Geología, Facultad CC. Experimentales, Campus El Carmen, 21071 Huelva, Spain*
[c] *Departamento Geología, Facultad Ciencias del Mar, UCA, 11510 Puerto Real, Cádiz, Spain*

Abstract

Accessory minerals are thought to play a key role in controlling the behaviour of certain trace elements such as REE, Y, Zr, Th and U during crustal melting processes under high-grade metamorphic conditions. Although this is probably the case at middle crustal levels, when a comparison is made with granulite-facies lower crustal levels, differences are seen in trace element behaviour between accessory minerals and some major phases. Such a comparison can be made in Central Spain where two granulite-facies terranes have equilibrated under slightly different metamorphic conditions and where lower crustal xenoliths are also found. Differences in texture and chemical composition between accessory phases found in leucosomes and leucogranites and those of melanosomes and protholiths indicate that most of the accessory minerals in melt-rich migmatites are newly crystallized. This implies that an important redistribution of trace elements occurs during the early stages of granulite-facies metamorphism. In addition, the textural position of the accessory minerals with respect to the major phases is crucial in the redistribution of trace elements when melting proceeds via biotite dehydration melting reactions. In granulitic xenoliths from lower crustal levels, the situation seems to be different, as major minerals show high concentration of certain trace elements, the distribution of which is thus controlled by reactions involving final consumption of Al-Ti-phlogopite. A marked redistribution of HREE–Y–Zr between garnet and xenotime (where present) and zircon, but also of LREE between feldspars (K-feldspar and plagioclase) and monazite, is suggested.

Keywords: Accessory minerals; Trace elements; Granulite facies; Spain

1. Introduction

The trace element behaviour of accessory and major minerals during metamorphism is a topic recently investigated by a combination of microanalytical techniques (electron microprobe, LA-ICP-MS) and textural studies (abundance, position, zoning via CL, SEM), and deserves attention because of its consequences in metamorphism and crustal melting. Knowledge of trace element geochemistry of mineral phases is also crucial to understanding the behaviour

* Corresponding author. Fax: +34-915442535.
E-mail address: granito@geo.ucm.es (C. Villaseca).

of REE–Y–Zr–Th–U during evolving metamorphic conditions and, especially, during crustal melting in high-temperature environments. The behaviour of accessory minerals and some other major minerals in granulite-facies conditions is poorly constrained and this contrasts with studies of accessory minerals in felsic magmatic series (e.g. Gromet and Silver, 1983; Wark and Miller, 1993; Hoskin et al., 2000). In some granulite-terranes, an increase in growth of monazite and zircon with increasing temperature and metamorphism has been described (Franz et al., 1996; Schaltegger et al., 1999; Rubbatto et al., 2001). In other granulite terranes, accessory minerals in peraluminous granulites have been consumed (xenotime), or their population has dramatically decreased with metamorphic grade (e.g. Ivrea-Verbano section, Bea and Montero, 1999; or in lower crustal xenoliths, Reid, 1990). A change appears to occur in the growth of trace minerals during the amphibolite to granulite facies transition (Bingen et al., 1996). Three major factors may explain the behaviour of accessory minerals during high-grade metamorphism: (i) textural position, (ii) solubility in melt, and (iii) behaviour in metamorphic reactions.

This work presents a detailed study of the behaviour of monazite, xenotime and zircon from peraluminous rocks (metapelites to felsic metaigneous lithologies) with increasing metamorphic grade. The samples form a middle-to-lower crustal section (from migmatite terranes to lower crustal xenoliths). We have investigated the combined textural and geochemical evolution of the main accessory minerals from well-characterized granulitic samples (Barbero, 1995; Barbero et al., 1995; Villaseca et al., 1999, 2001; Martín Romera et al., 1999).

2. Geological outline of the study area

The migmatitic terranes of central Spain reached peak metamorphic conditions during the second Hercynian tectonothermal stage (M_2) of low-P/high-T conditions following exhumation (Barbero and Villaseca, 2000). Two areas are representative of these migmatitic terranes: an anatectic area in the Guadarrama mountains (Sotosalbos) and the Anatectic Complex of Toledo (ACT). In Sotosalbos, the low-pressure migmatites and related anatectic granites have cordierite and biotite as mafic minerals and their peak metamorphic conditions have been estimated to be around 750 ± 50 °C and 4–5 kb (Martín Romera et al., 1999). The closely related Peña Negra anatectic area shows similar petrogenetic characteristics (Bea et al., 1994; Pereira and Rodriguez Alonso, 2000). In contrast, the ACT migmatites are characterized by garnet and cordierite as mafic minerals (biotite is more scarce) and their peak metamorphic conditions have been estimated to be around 800 ± 25 °C and 4–6 kb (Barbero, 1995).

The third sample of granulitic material is a suite of lower crustal xenoliths. Permian post-Hercynian ultrabasic alkaline dykes carry a varied population of peraluminous granulitic xenoliths with mineral paragenesis indicative of equilibrium conditions (900–950 °C and 9–11 kb) close to the base of the crust (Villaseca et al., 1999).

Although outcropping continuity between the groups of samples (migmatite terranes and xenoliths) is missing, all of the granulitic rocks originated during the same orogenical cycle and are composed of equivalent peraluminous lithotypes, i.e., metasedimentary and felsic metaigneous rocks (Villaseca et al., 1999, 2001). Hence, an evaluation of the consequences of the increase in metamorphic conditions on accessory mineral assemblages can be established.

The age of granulitic metamorphism in this crustal section is unresolved. U–Pb monazite ages from high-grade orthogneisses in the Guadarrama sector give 337 ± 2 Ma as a probable age of the M_2 metamorphic peak (Escuder Viruete et al., 1998). In the Toledo sector, U–Pb monazite ages from anatectic granitoids give a younger but more discordant value of 310 ± 1 Ma (Barbero and Rogers, 1999). More speculative is the age of the granulite-facies metamorphism of the xenolith suite but their trapping by late-Hercynian alkaline lamprophyres (283 ± 30 Ma in age, after Bea et al., 1999) has permitted a natural sampling of the Hercynian lower crust. Although there is an important diachronism in the age of high-grade metamorphism of the studied samples, the different granulitic assemblages presumably belong to the Hercynian metamorphic peak at different crustal levels, as this diachronism is similar to that obtained in tectonothermal models (e.g. Gerdes et al., 2000).

3. Petrographic features of migmatites, granulites and related granites

A detailed petrographic description of the materials considered in this work can be found in several previous papers (Barbero et al., 1995; Villaseca et al., 1998, 1999, 2001), thus, only a brief summary is given here.

3.1. Sierra de Guadarrama migmatites and anatectic granites

In the Sotosalbos area, cordierite-bearing granitoids are related to partially migmatized orthogneisses. These anatectic granitoids locally contain cordierite-rich nodules, corroded augen (megacrysts) of K-feldspar, and orthogneissic xenoliths, suggestive of their derivation from those felsic metaigneous lithotypes (see also Martín Romera et al., 1999). The Sotosalbos granitoid also shows sporadic mm-scale biotite-rich enclaves that resemble regional melanosomes. Related cordierite-bearing migmatites usually display mafic nodules rimmed by leucocratic haloes that overprint the host-rock foliation. Some migmatites are localized in narrow shear zones and provide evidence that melt segregation occurred. Typical mesosome–leucosome pairs are rare as are mafic selvedges. In general, in situ residual granulitic material is difficult to find in the Guadarrama area.

Table 1 gives the modal composition (in vol.%) of the different units of this migmatitic area. The *leucosomes* consist dominantly of K-feldspar with quartz, plagioclase, minor biotite and some cordierite or almandine–spessartine garnet (Table 1). *Melanosomes* have a more mafic character than the regional orthogneisses, being rich in biotite, plagioclase and quartz, and also in accessory minerals. K-feldspar and cordierite are rare. The *Sotosalbos granite* is a medium-grained equigranular rock consisting of quartz, plagioclase, K-feldspar, biotite and cordierite with accessory tourmaline. Cordierite contains minor inclusions of biotite and sillimanite. Feldspar also contains needles of sillimanite. The scarce *biotite-rich xenoliths* resemble biotite-rich folia of the augen-gneisses. The most striking feature of these xenoliths is the high content of accessory minerals that are usually enclosed in biotite or plagioclase (Table 1).

3.2. Anatectic complex of Toledo

In the Toledo Complex (ACT), the metasedimentary material mostly exhibits a stromatic-banded migmatitic structure. The *melanosomes* are mainly composed of cordierite, sillimanite, and garnet, with minor biotite, plagioclase, spinel and ilmenite (kinzigites) (Table 1). Well-developed coronas of cordierite appear around garnet. Cordierite commonly contains inclusions of quartz, sillimanite, biotite, ilmenite, and spinel. Biotite is scarce and is usually interstitial to cordierite, suggesting that biotite dehydration melting reactions had almost run to completion (Barbero, 1995). The *leucosomes* are characterized by a larger grain-size than the melanosomes. They are essentially composed of K-feldspar and quartz, with subordinate proportions of plagioclase (Table 1). The presence of large rounded garnet porphyroblasts (up to 7–8 cm) with inclusions of sillimanite, biotite, and quartz is very characteristic. Accessory minerals are rare in comparison to the melanosomes. Two types of leucosomes have been distinguished in this area on the basis of their geochemistry (Villaseca et al., 2001): (i) normal or N-type leucosomes with low-REE (and Th–Y–Zr) contents and a positive chondrite-normalized Eu anomaly, and (ii) a high-REE leucosome (enriched or E-type) with a negative Eu anomaly.

Related anatectic leucogranites (Cervatos-type) and restite-rich granitoids (Layos-type) appear in the ACT (Barbero et al., 1995). The *Layos granite* is a suite ranging from quartz-rich tonalite to melamonzogranite, characterized by a high modal proportion of cordierite (up to 30%) (Table 1). The *Cervatos leucogranites* outcrops as vein-like or dyke-like concordant sheets, or elongated massifs, in most cases associated with the Layos granites. These leucogranites have a modal eutectic composition and display centimetre-scale layering consisting of garnet-, cordierite- or very scarce biotite-bearing leucogranites. Essentially all of the mineral phases in both the anatectic granites and in the migmatitic granulites of the ACT have similar compositions (Barbero, 1995).

3.3. Granulitic xenoliths from lower crustal levels and late Hercynian granites

Three types of lower crustal granulites have been described by Villaseca et al. (1999) in the Sierra de

Table 1
Granulite mineral assemblages

Modal analyses (vol%) by point counting methods

	Anatectic Complex of Sotosalbos							Anatectic Complex of Toledo					Lower crustal xenoliths	
	Orthogneiss	Bt-rich enclave	Melanosome	Sotosalbos granite	N-leucosome	N-leucosome	Leucogranite	Melanosome	Layos granite	N-leucosome	E-leucosome	E-Cervatos leucogranite	Pelitic	Felsic metaigneous
Sample	60870	100562	101637	100563	101638	102181	102183	93198	89103	93201	93197	81926	77750	99185
Quartz	26	1	17	32	19	29	20	18	22	24	22	34	21	28
K-feldspar	27	–	–	19	46	52	49	27	15	60	59	27	33	24
Plagioclase	15	1.2	17	26	31	15	27	5	18	8	5	20	–	6
Biotite	25	73	42	10	3	1.5	3	21	19	0.8	3	3	–	0.1
Garnet	1	–	–	–	–	Tr	–	5	–	2	5	7	30	40
Cordierite	Tr	–	9.5	7	Tr	–	Tr	22	23	5	6	8	–	–
Sillimanite	6	21	12	0.5	–	–	–	0.3	0.2	–	–	0.4	12	–
Opaques	Tr	0.4	0.9	0.4	–	–	Tr	1.3	0.2	0.2	0.3	0.3	0.1	0.3
Apatite	Tr	0.6	0.6	0.4	Tr	Tr	Tr	Tr	Tr	Tr	Tr	Tr	Tr	Tr
Other accs.	Tr	1.1	0.3	0.1	Tr	Tr	Tr	Tr	0.1	Tr	Tr	0.3	Tr	0.2
Tourmaline				3										
Rutile													1.6	1.5
Others		Ms (2%)		Ms (1.5%)		Ms (2%)	Ms (1%)	Spl (Tr)	Ms (3.7%)					

Number of accessory crystals (per cm^2) by SEM counting

				100560					93193				95148	99185
Apatite	25	97	18	10	1			18	22	1	3	1	–	2
Monazite	55	164	68	16	8			48	53	4	29	3	9	–
Zircon	56	454	200	46	4			170	156	19	44	17	55	21
Xenotime	11	10	–	6	1			4	4	–	–	–	–	–

Guadarrama. They are rare felsic to intermediate charnockites (<0.01 vol.%), metapelites (5 vol.%) and common felsic meta-igneous types (95 vol.%). These granulites are granoblastic and many exhibit small-scale banding marked by garnet-rich bands alternating with felsic-rich layers, but clear migmatite structures are not evident. The felsic meta-igneous granulites are quartzo-feldspathic garnet-bearing types, sometimes with orthopyroxene or sillimanite as accessories. The pelitic xenoliths have prismatic sillimanite as a major mineral (>8 vol.%) (Table 1).

The granulitic xenoliths are interpreted as the residual counterpart of the Hercynian granitic batholith of the Spanish Central System (SCS) (Villaseca et al., 1999). The batholith is composed of dozens of plutons, mainly monzogranitic in modal composition, intruded during a time span of around 40 Ma (Villaseca et al., 1998). These granites intrude and generate typical contact aureoles in the exhumed middle-crust migmatite terranes previously described. A detailed study of the mineralogy, geochemistry and petrogenesis of these Hercynian peraluminous granites can be found in Villaseca et al. (1998) and Villaseca and Herreros (2000).

4. Analytical methods

Modes of the rocks from the migmatite terranes and xenoliths were derived from point counting of thin sections. More than 1200 points were counted in each 24 × 46-mm thin section. Because of the small size and difficulty in optical distinction, accessory mineral counting in a small area (1 cm^2) was performed using a scanning electron microscope (SEM) (Table 1). Electron microprobe analyses were carried out on thin sections at the Microscopía Electrónica CAI, University Complutense of Madrid. Before microchemical analyses, most of the thin sections were studied using a SEM equipped with an energy-dispersive spectrometric system. This method unambiguously distinguished monazite from zircon and xenotime. Backscattered electron images were used as a guide during microprobe analysis. Some zircon and accessory concentrates from the three granulite sectors were also obtained using standard heavy liquid and magnetic separation techniques, but most of the textural study was based on the thin sections.

Major element concentrations of accessory minerals (monazite, xenotime, zircon) were obtained by wavelength dispersive electron microprobe JEOL Superprobe JXA 8900-M equipped with four crystal spectrometers. Operating conditions were between 15 and 20 kV, and a beam current of approximately 20 to 50 nA in spots of 2–5 μm in diameter. About 24 min was necessary for each spot analysis. Absolute abundances for each element were determined by comparison with synthetic REE phosphates prepared by Jarosewich and Boatner (1991), and natural minerals for Zr, Y, U and Th. Error limits for each element depend strongly on the absolute concentration in each phase but are significant for the <1 wt.% level (with error >10%). Concentrations below 0.2 wt.% are merely qualitative.

Laser ablation-ICP-MS analyses of garnets and feldspars were obtained using a Hewlett Packard HP4500 Coupled Plasma-Mass Spectrometer (ICP-MS) equipped with a CETAC LSX-100 laser ablation microprobe (LAM) at the University of Huelva. Operating conditions were optimised prior to analysis by using a 10-ppb solution of ^{7}Li, ^{89}Y and ^{205}Tl. Plasma Ar flow rate was 15.00 l min^{-1}; gas carrier and auxiliary flow rate were 1.25 and 0.5 l min^{-1}, respectively. Ablation craters were made using a Nd:YAG laser with 266-nm wavelength operating in Q-switch mode. The laser beam was optimised to produce ablation craters with diameters smaller than 70 μm. Selected isotopes were acquired by the Time-Resolved Analysis (TRA) procedure, which allows the variation in concentration to be known at any time. In this way, the presence of either compositional zonation or mineral inclusions can be monitored (Longeritch et al., 1996). Corrections and final calculations of concentrations were made following Longeritch et al. (1996), using ^{29}Si as an internal standard. Calibration was performed using the glass standard NIST RSM 612 which was analyzed four times before and two times after each run of 22 samples. The precision and accuracy were estimated using the ATHO-G standard, a MPI-DING reference glass (Jochum et al., 2000). Precision is estimated to be between 2% and 10% for most of the analyzed trace elements. In general, an accuracy of ± 18% can be claimed for the LA-ICP-MS analyses, but agreement of measured

Table 2
Sample suite accessory mineral assemblage

Samples	Description	Sample suite	Monazite (mnz)	Zircon (zrn)	Xenotime	Ap	Ilm	Fe–S	Other	Inclusions in zircon
100942-5	orthogneiss	Sotosalbos	I–III? (fels, bt, m)	B–C (bt, fels)	II (bt, qrz)	X	X	X		
60870–62458	orthogneiss	Sotosalbos	I (bt, fels, m)	B–C?–D (bt, m)	I (fels)	X	X	X	Gr	
102175	melanosome	Sotosalbos	III (fels, m)	B (bt, m)		X	X	X		ap, bt
100562	bt-rich enclave	Sotosalbos	I–III (bt, ap, m)	B?–C (bt, m)	I (bt, m)	X	X	X	Si–Y–REE carbonate?	
101638–102181	leucosome	Sotosalbos	I–III (bt, fels, m)	A?–C–D (fels–m)	II (m)	X	X			
102183	leucogranite	Sotosalbos	II–III (bt, fels, m)	C (bt, m)	II (bt)	X	X			
100560-3	granitoid	Sotosalbos	II–III (fels, m)	A?–B–C (bt, fels, m)	I	X	X	X	Cheralite	
100940-1-3	granitoid	Sotosalbos	III (bt, fels, m)	A–B–C (bt, fels, m)		X	X			qrz, pl, bt, sil, ap
87085–93198	melanosomes	Toledo	I–III (m, fels, grt, crd)	C (m, fels, bt, crd)	I	X	X	X		
93197	leucosome	Toledo	I–III (fels, bt, m)	C–D (fels, bt, grt, m)		X	X	X		mnz
81925-6-87202	leucogranite	Toledo	I–III (fels, bt, m)	B–C–D (fels, bt, m)		X	X	X		
93193	Layos granitoid	Toledo	I–III (fels, bt, m)	A–B–C–D (fels, bt, m)	I (m, bt)	X	X	X		qtz, sil
77750/U-46	pelitic	Xenoliths	I–III (qtz, fels, m)	B–C–D (qtz, fels, sil, m)		X	X	X	Rt, Gr	sil
81846–95151	felsic	Xenoliths	I–III (fels, m)	A?–C–D (fels, grt, m)		X	X	X	Rt	
95148–99185	felsic	Xenoliths	III (fels, grt, sil, m)	B–C–D (fels, grt, sil, m)		X	X	X	Rt	

X: mineral identified in sample.
(bt, grt, crd...): accessory present as inclusion in biotite, garnet, cordierite.
fels: felsic mineral (feldspar or quartz).
m: accessory present as matrix (or interstitial) mineral.
?: indicates tentative identification only.
Other mineral abbreviations after Kretz (1983).

and expected values was better than 10% for most of the REEs (Appendix A). Analyses of some metals (Cr, Ni, V) are strictly qualitative as they show larger inaccuracies. More details on LA-ICP-MS analytical techniques are in Otamendi et al. (2002).

5. Texture of the accessory phases with increasing metamorphic grade

Detailed SEM and microprobe analyses revealed that REE–Y–Th–U–Zr-rich accessories in granulites

Fig. 1. BSE images showing petrographic features of accessory minerals. Scale bar in A to E is 10 μm. Scale bar in F is 20 μm, in G is 100 μm, and in H is 50 μm. (A) Complex and irregular zoning in type-III monazite with bright high Th (low U) core and high U (low Th) rim. This chemical zoning is the reverse of the common zoning in leucocratic migmatites. Sotosalbos granite 100941 (analyses 44 to 47 in Table 3). (B) Idiomorphic zoning in type-II monazites showing also an increase in U contents from core to rim. Sotosalbos granite 100560 (analyses 11 and 10 in Table 3). (C) Complex zoning in type-III monazite showing bright interstitial cheralite (Cher). In this grain, chemical zoning is from low Th–U core towards higher Th–U rim. Sotosalbos granite 100563 (analysis 17 in Table 3). (D) Type-II xenotime in leucosome 101638 from Sotosalbos area. (E) Unzoned xenotime crystal (type-I) partially surrounding zircon. Layos granite 93193. (F) Rounded sillimanite inclusion in unzoned zircon (type-D). Lower crustal granulitic xenolith 77750. (G) Type-A zircons with plagioclase inclusions in Sotosalbos granite 100943. (H) Type-B zircons in Layos granite (M-3 concentrate).

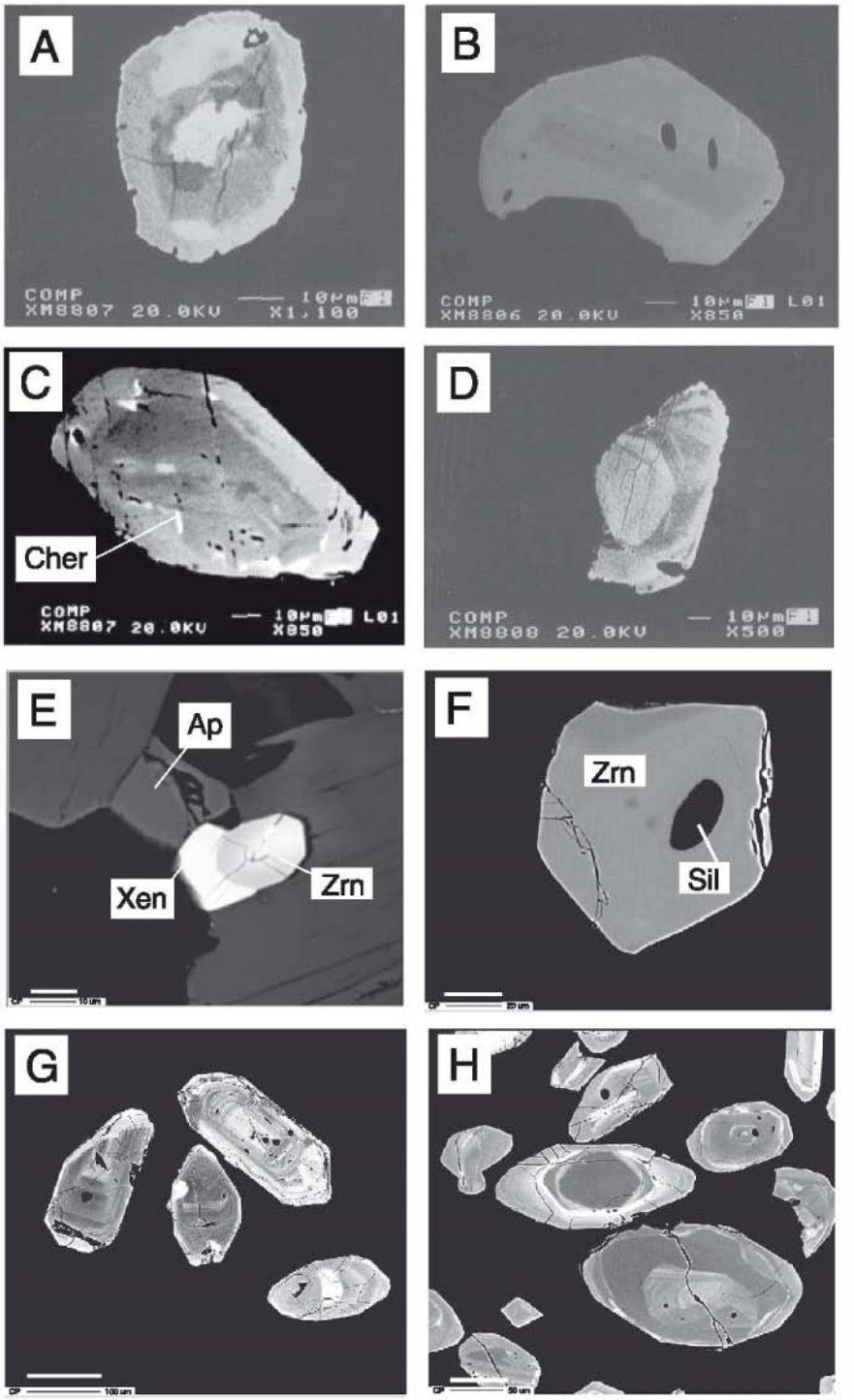
A
COMP
XM8807 20.0KV
X1,100
B
COMP
XM8806 20.0KV
X850
L01
C
Cher
COMP
XM8807 20.0KV
X850
L01
D
COMP
XM8808 20.0KV
X500
E
Ap
Xen
Zrn
F
Zrn
Sil
G
H

from these migmatite terranes are apatite, zircon, monazite and more rarely, xenotime (Table 1). In lower crustal xenoliths, only rare apatite in some enclaves, zircon and scarce monazite, are found. The general trend of a decrease in abundance of accessory minerals in peraluminous granulites with increasing metamorphic grade is similar to that found by Bea and Montero (1999) in the Ivrea-Verbano section or by Pyle and Spear (1999) with respect to xenotime in pelites. This contrasts with the general trend of increased growth of accessory minerals usually found in peraluminous lithologies from greenschist to amphibolite/granulite facies transition (Franz et al., 1996; Rubbatto et al., 2001). In general, accessory phases in the studied samples appear as isolated crystals not defining clusters or groups as found in felsic igneous rocks (e.g. Wark and Miller, 1993) or in accessory-rich metamorphic rocks (e.g. Pan, 1997). They usually appear as

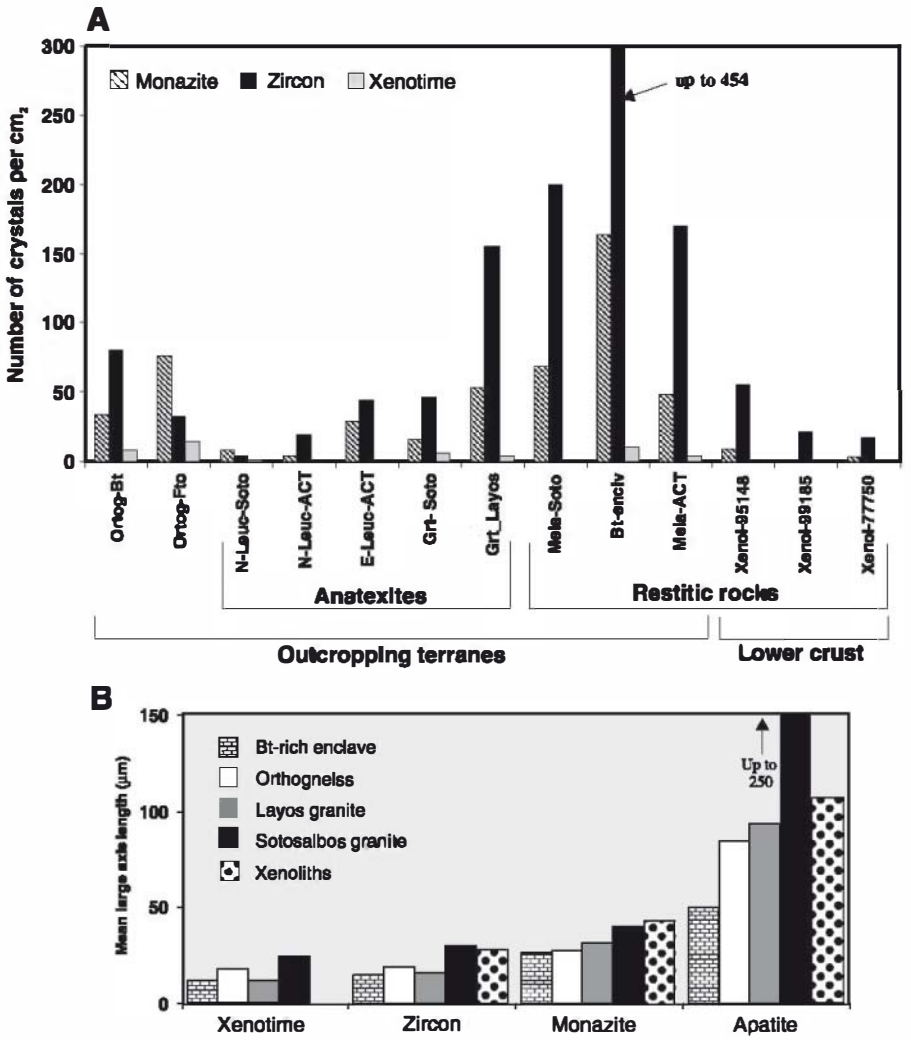

Fig. 2. Variations in modal amounts and average large axis length of accessory minerals in granulitic samples. (A) Modal amounts of monazite, zircon and xenotime in melt-rich migmatites (anatexites), residuum-rich migmatites and regional orthogneisses. Xenolith samples show a marked decrease in abundance of accessory minerals with respect to restitic migmatites from granulite terranes. Xenotime is absent in xenoliths and monazite is very scarce in some thin sections. Data set from Table 1. (B) Average large axis length of accessory phases in granulitic samples showing an increase in size from the smallest (xenotime) towards the largest (apatite) crystals irrespectively of the lithotype.

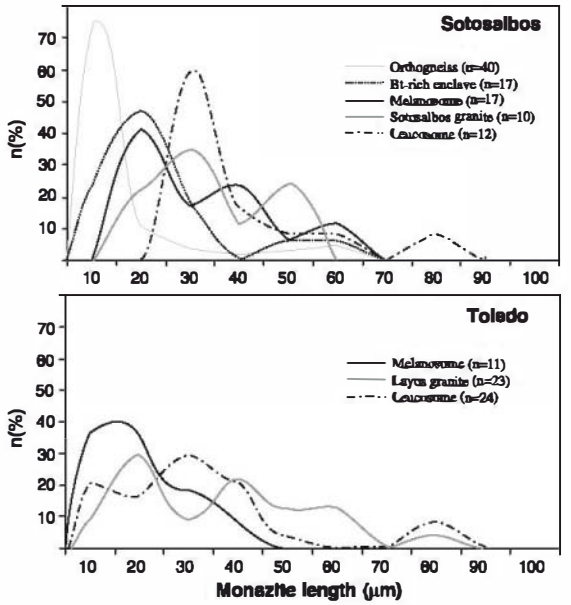

Fig. 3. Plots showing monazite crystal size distribution in samples from the studied migmatite terranes. A larger crystal size and a decreased overall monazite frequency is characteristic of leucocratic migmatites, best displayed in monazites from the Sotosalbos complex. The legend shows the number of measured monazite crystals.

interstitial or matrix minerals but are also inclusions in the major phases (Table 2). Nevertheless, some crystals of accessory minerals occasionally appear grouped, mostly in some accessory-rich samples (Fig. 1E).

5.1. Apatite

Apatite is the largest accessory mineral (>95 µm in melt-rich migmatites) (Fig. 2). Its proportion diminishes strongly from samples of granulite terranes to those of granulitic xenoliths (Table 1). There is also a modal decrease from residuum-rich to melt-rich migmatites. Monazite may surround apatite crystals or be included in larger apatites. More rarely, xenotime and zircon are situated at apatite rims (Fig. 1E). Due to their larger size, although there are few apatite crystals in a 1-cm^2 section (Table 1), they usually constitute the most abundant accessory mineral.

5.2. Monazite

The modal amount of *monazite* diminishes significantly from migmatites of granulite terranes to granulitic xenoliths (Table 1, Fig. 2). There is also a marked decrease of monazite abundance between leucosome and melanosome pairs, as usually described in migmatite terranes (e.g. Watt et al., 1996; Nabeleck and Glascock, 1995; Bea and Montero, 1999). A maximum concentration in biotite-rich enclaves of Sotosalbos granitoid is observed, in agreement with the

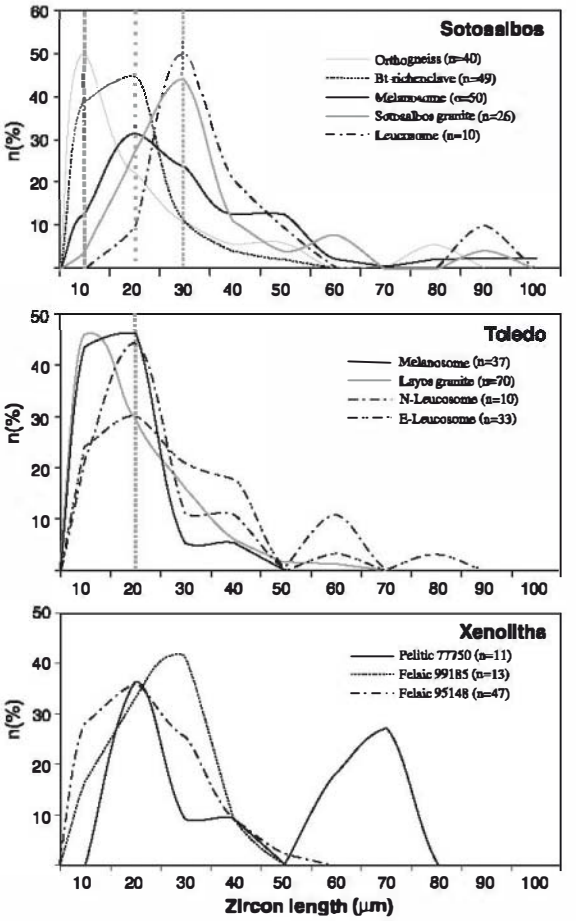

Fig. 4. Plots showing zircon crystal size distribution from studied samples. As for monazites, zircons have a larger crystal size and a higher heterogeneity of sizes in leucocratic migmatites. In the Sotosalbos plot, vertical line at 30 µm approximates the modal zircon length in melt-rich migmatites (e.g. leucosomes), whereas 20 µm is the modal zircon length in melt-poor migmatites (bt-rich enclave and melanosome), and 10 µm is the modal zircon length in regional orthogneisses. In the plot of Toledo zircons, vertical line at 20 µm approximates the mode in melt-rich migmatites whereas restite-rich migmatites have modal zircon lengths more displaced towards lesser size (being 13 µm in average). n=number of measured zircon crystals.

Table 3
Representative EMP analyses of monazites

Sample	Anal			La_2O_3	Ce_2O_3	Pr_2O_3	Nd_2O_3	Sm_2O_3	Gd_2O_3	Dy_2O_3	Er_2O_3	Yb_2O_3	Y_2O_3	ThO_2	UO_2	P_2O_5	SiO_2	CaO	Total
Sotosalbos Complex																			
100560	Granite	10	r	13.12	27.40	2.73	11.85	1.92	2.36	0.59	0.30	0.11	2.34	4.48	2.15	30.78	0.06	1.34	101.79
100560	Granite	11	c	13.76	27.92	2.88	12.58	1.78	2.33	0.53	0.28	0.12	2.46	4.01	0.29	30.15	0.08	0.92	100.29
100941	Granite	44	bc	13.60	25.37	2.70	9.20	1.27	1.86	0.47	0.29	0.13	1.20	11.73	0.94	27.34	1.70	1.31	99.53
100941	Granite	47	r	13.03	26.91	3.15	11.59	2.11	2.15	0.62	0.19	0.12	2.16	3.72	4.34	30.19	0.05	1.56	102.32
100563	Granite	17	Cheralite	8.74	17.23	2.07	8.44	1.25	1.42	0.30	0.32	0.15	1.43	29.54	2.49	21.96	5.96	1.44	103.07
100563	Granite	20	r	13.39	25.92	2.97	11.50	2.09	2.33	0.91	0.39	0.15	2.92	4.43	2.40	30.18	0.11	1.35	101.37
100940	Granite	22	c	11.91	26.00	3.10	12.32	1.97	2.48	0.79	0.37	0.09	1.94	5.47	0.62	30.78	0.19	1.13	99.67
100940	Granite	23	r	11.63	25.90	3.06	12.31	1.97	2.17	0.86	0.34	0.15	1.95	5.53	0.68	31.04	0.20	1.13	99.50
60870	Orthogneiss	15	unz	11.64	26.04	2.97	11.87	2.00	2.34	1.02	0.47	0.17	4.12	6.43	0.70	30.81	0.20	1.35	102.71
60870	Orthogneiss	1	c	9.11	24.55	3.00	10.98	2.40	2.24	0.96	0.43	0.20	3.43	9.53	1.91	30.20	0.16	2.44	102.10
100942	Orthogneiss	44	unz	11.87	25.58	2.80	11.45	1.99	2.17	0.61	0.29	0.13	2.20	6.46	1.57	28.36	0.20	1.69	97.69
100942	Orthogneiss	53	unz	13.05	26.46	2.73	11.56	1.94	2.36	0.72	0.31	0.13	2.36	5.26	2.34	30.96	0.17	1.47	102.06
62458	Orthogneiss	20	unz	12.58	27.46	3.11	12.54	2.04	2.26	0.82	0.36	0.14	3.38	4.87	0.46	31.30	0.18	1.08	103.05
62458	Orthogneiss	23	unz	12.97	27.67	3.09	12.05	2.05	2.31	0.58	0.25	0.07	2.01	4.96	2.01	31.34	0.04	1.52	103.39
100945	Orthogneiss	19	c	10.90	23.81	2.82	11.50	1.99	2.29	1.03	0.44	0.13	4.31	7.38	1.98	28.92	0.73	1.24	100.12
101638	Leucosome	25	i	13.29	25.82	2.77	10.92	1.75	2.14	0.82	0.44	0.10	2.93	4.97	3.18	28.98	0.11	1.60	100.38
101638	Leucosome	26	bi	13.23	26.66	2.75	10.94	1.73	2.19	0.43	0.38	0.08	2.33	7.40	1.92	28.78	0.95	1.13	101.34
101638	Leucosome	34	bc?	12.77	24.99	2.59	10.47	1.59	2.22	0.77	0.45	0.12	3.18	5.79	3.69	30.00	0.12	1.88	101.22
101638	Leucosome	45	unz	13.74	27.01	2.79	10.75	1.37	2.22	0.53	0.36	0.11	2.06	6.74	1.22	28.56	0.95	1.12	99.85
102183	Leucogranite	31	c	12.66	25.22	2.92	11.13	1.95	2.35	0.69	0.49	0.15	1.82	5.20	3.45	30.78	0.10	1.72	101.23
102183	Leucogranite	32	i	13.13	26.21	2.89	11.39	1.91	2.47	0.60	0.38	0.10	1.71	4.68	2.58	29.24	0.11	1.46	99.46
102183	Leucogranite	30	c	12.44	25.22	2.86	10.93	2.04	2.16	0.63	0.53	0.12	1.63	4.71	4.74	29.79	0.13	1.86	100.39
102183	Leucogranite	29	r	12.33	24.97	2.83	11.17	2.06	2.45	0.67	0.54	0.16	1.87	4.41	3.94	29.11	0.07	1.65	98.87
102181	Leucosome	8	c	10.09	24.23	2.95	11.03	2.34	2.32	0.77	0.47	0.10	1.56	8.56	2.78	29.42	0.21	2.34	99.82
102181	Leucosome	9	r	12.65	25.64	3.04	12.30	1.98	2.25	0.61	0.52	0.10	1.37	5.37	1.64	29.51	0.10	1.54	99.21
102178	Leucosome	16	unz	13.52	26.62	3.18	13.55	1.85	1.88	0.41	0.47	0.10	1.53	4.80	0.25	29.71	0.15	1.00	99.36
102178	Leucosome	15	unz	13.59	26.15	2.87	11.51	1.94	2.23	0.62	0.52	0.10	1.72	4.93	1.55	29.85	0.11	1.43	99.58
102175	Melanosome	29	c	13.39	27.31	3.02	12.63	1.73	2.03	0.64	0.49	0.13	2.95	4.62	0.40	28.92	0.16	1.08	99.92
102175	Melanosome	30	r	12.40	26.33	2.90	12.54	1.79	2.23	0.78	0.49	0.12	3.66	5.47	0.55	28.96	0.24	1.24	100.11
102175	Melanosome	31	c	13.42	27.08	2.92	13.14	1.80	2.13	0.58	0.49	0.11	2.73	4.27	0.54	29.17	0.10	1.06	100.00
102175	Melanosome	32	r	13.16	26.97	3.03	13.00	1.76	2.17	0.58	0.46	0.11	3.12	4.78	0.40	29.03	0.17	1.02	100.26
100562	Bt-rich enclave	10	c	13.28	27.33	3.06	13.05	1.71	2.00	0.46	0.51	0.08	1.73	4.49	0.67	29.11	0.09	1.25	99.23
100562	Bt-rich enclave	11	r	13.06	26.52	3.06	12.76	1.92	2.15	0.70	0.53	0.09	2.73	3.11	1.43	29.36	0.07	1.08	99.12
100562	Bt-rich enclave	18	unz	13.54	27.55	3.04	12.79	1.84	2.14	0.64	0.46	0.15	3.01	3.40	1.30	30.42	0.05	1.01	101.90

Toledo Complex																		
87085	Kinzigite	2	in-grt	13.24	26.04	2.53	10.02	3.51	3.13	0.88	0.00	0.61	3.17	4.47	0.53	30.02	0.15	1.08	99.81
87085	Kinzigite	4	in-crd	14.39	28.63	2.87	10.90	3.56	2.90	0.00	0.00	0.02	0.16	4.82	0.58	29.77	0.42	0.87	100.29
87085	Kinzigite	12	c	14.19	27.50	2.21	9.86	3.59	3.26	0.69	0.39	0.40	2.55	2.45	0.51	30.11	0.13	0.68	98.99
87085	Kinzigite	13	r	14.78	28.81	2.41	10.52	3.70	2.95	0.18	0.65	0.30	0.62	2.46	0.43	29.61	0.11	0.58	98.46
93198	Melanosome	1		13.75	30.24	nd	10.31	1.80	1.60	0.67	0.50	0.14	2.17	4.30	0.97	31.78	0.10	1.13	100.06
93198	Melanosome	7		14.98	31.59	nd	10.45	2.03	1.68	0.46	0.35	0.14	1.36	4.03	0.80	31.63	0.08	0.98	100.68
93198	Melanosome	9		13.56	29.63	nd	9.87	2.02	2.21	1.04	0.34	0.10	2.59	3.84	0.68	30.28	0.15	1.03	97.79
93198	Melanosome	10		13.46	29.42	nd	9.87	1.95	1.65	0.95	0.37	0.10	2.15	4.20	1.02	29.98	0.17	1.10	96.65
81926	Leucogranite	1	c	12.95	29.57	nd	11.93	2.26	2.24	0.72	0.25	0.09	1.34	3.56	1.96	30.26	0.04	1.08	98.74
81926	Leucogranite	3	r	15.18	32.41	nd	11.63	1.62	0.66	0.20	0.29	0.08	0.41	5.87	0.98	29.79	0.08	1.43	100.89
81926	Leucogranite	16	c	15.52	32.71	nd	11.31	1.51	0.77	0.15	0.29	0.10	0.43	6.00	0.98	30.13	0.09	1.47	101.72
81926	Leucogranite	17	r	14.98	31.05	nd	10.49	1.10	1.05	0.42	0.35	0.12	1.34	5.64	1.22	29.84	0.08	1.44	99.47
87202	Leucogranite	49	c	13.45	27.62	2.21	10.44	1.60	2.09	0.35	0.18	0.04	1.55	6.52	1.49	30.22	0.18	1.75	100.00
87202	Leucogranite	51	r	13.47	28.22	2.12	10.82	1.74	2.02	0.18	0.03	0.02	0.68	7.51	1.31	30.13	0.32	1.80	100.40
87202	Leucogranite	52	c	12.41	27.65	2.18	11.68	1.64	1.67	0.32	0.16	0.07	0.54	9.00	0.67	29.52	0.64	1.69	100.03
87202	Leucogranite	53	r	15.03	28.89	1.82	9.10	1.19	1.90	0.38	0.00	0.00	0.92	6.13	3.06	30.08	0.13	1.91	100.69
93197	E-leucosome	32	c	11.15	26.36	2.43	11.38	1.91	1.92	0.17	0.19	0.07	0.71	9.93	1.14	29.26	0.36	2.26	99.42
93197	E-leucosome	33	r	13.21	28.43	2.19	11.15	2.06	2.52	0.42	0.09	0.13	0.81	5.80	1.08	29.21	0.30	1.51	98.99
93197	E-leucosome	46	c	13.91	28.67	2.11	11.04	1.88	2.44	0.39	0.31	0.12	1.43	5.01	0.77	29.45	0.15	1.22	99.04
93197	E-leucosome	47	i	10.91	25.64	2.30	10.91	2.08	1.96	0.48	0.16	0.11	1.20	8.61	2.94	29.59	0.23	2.38	99.75
93197	E-leucosome	48	r	13.24	27.36	1.97	10.55	1.79	2.14	0.51	0.15	0.05	1.99	5.74	1.22	29.52	0.10	1.60	98.09
93193	Layos granite	5	c	13.62	29.27	2.20	11.92	2.15	2.62	0.61	0.22	0.13	1.61	3.45	0.96	29.91	0.06	0.94	99.91
93193	Layos granite	6	r	13.27	28.18	2.08	11.19	1.59	2.23	0.35	0.06	0.03	0.70	6.48	2.03	30.63	0.07	1.85	100.79
93193	Layos granite	16	c	13.29	28.94	2.24	11.34	1.38	1.65	0.12	0.11	0.00	0.43	8.56	0.41	28.50	1.00	1.24	99.24
93193	Layos granite	17	r	11.13	24.26	1.76	9.74	1.40	2.13	0.56	0.17	0.11	2.14	4.73	1.51	27.26	5.72	1.42	94.25
Xenoliths																			
77750	Pelitic	5	c	13.44	29.85	2.80	11.33	2.78	2.10	0.00	0.00	0.29	0.04	5.02	0.70	29.27	0.65	0.87	99.52
77750	Pelitic	6	r	13.67	29.37	2.71	10.73	2.49	2.05	0.04	0.00	0.18	0.08	6.02	0.39	28.56	0.62	0.89	98.26
77750	Pelitic	8	unz	13.34	29.43	2.67	11.22	2.79	1.99	0.00	0.00	0.04	0.03	4.72	0.89	29.56	0.45	0.89	98.31
U-46	Pelitic	1	unz	14.80	34.09	0.73	12.20	1.40	0.61	0.00	0.04	0.15	0.01	5.26	0.31	30.06	0.21	1.13	101.00
U-46	Pelitic	2	unz	15.52	33.64	0.00	10.63	1.64	0.67	0.01	0.30	0.12	0.04	5.29	0.37	30.54	0.19	1.06	100.13
81846	Felsic	24	unz	15.31	31.85	3.78	13.70	2.32	1.93	0.15	0.05	0.08	0.24	1.01	0.24	30.80	0.06	0.31	101.90
81846	Felsic	29	unz	10.74	27.25	3.70	16.45	2.58	0.95	0.00	0.11	0.07	0.16	6.51	0.73	29.61	0.15	1.44	100.55
81846	Felsic	30	unz	9.15	23.17	3.30	14.41	2.15	0.40	0.09	0.08	0.13	0.09	13.70	0.94	29.61	0.48	2.79	100.55
95148	Felsic	10	r	8.52	23.83	3.68	16.22	1.34	0.08	0.09	0.10	0.05	0.08	15.24	1.20	26.08	2.46	1.27	100.29
85148	Felsic	9	c	8.54	23.31	3.70	16.31	1.56	0.00	0.02	0.08	0.05	0.02	15.59	1.29	25.80	2.23	1.26	99.82
99185	Felsic	1	unz	15.33	28.87	3.31	12.12	1.81	2.21	0.04	0.06	0.11	0.23	4.83	1.20	30.31	0.20	0.83	101.42
95151	Felsic	16	c	14.13	27.80	3.38	13.68	1.99	1.52	0.26	0.06	0.03	0.36	3.99	0.97	29.19	0.15	0.90	98.38
95151	Felsic	17	r	10.41	24.62	3.49	15.37	1.80	0.52	0.06	0.07	0.07	0.09	10.25	0.81	29.73	0.50	1.93	99.73

r = rim, c = core, i = intermediate zone, unz = unzoned crystal, b = bright, in-mineral = included mineral.

general observation of biotite being the main host mineral for accessory phases in migmatite terranes (e.g. Bea et al., 1994; Johannes et al., 1995). Nevertheless, in the ACT terrane where biotite was nearly consumed during dehydration reactions (Barbero, 1995), the accessories are distributed elsewhere in the major minerals of the migmatite, especially in those generated in the incongruent melting reactions i.e., K-feldspar, cordierite and garnet (Table 2). This has been observed in other migmatite areas (e.g. Watt et al., 1996). Monazite has few inclusions, and only biotite, apatite and zircon have been identified.

The average grain size of monazite is approximately 30–100 μm in diameter and remains similar in all the studied granulites, in contrast to other crustal sections where its grain-size decreases with metamorphic grade (Bea and Montero, 1999) (Fig. 2B). In detail, some slight contrasts in shape and size appear in monazites from the migmatite terrane samples. Monazite from the anatectic granitoids of Sotosalbos are slightly more idiomorphic and larger than in the surrounding orthogneisses or restitic counterparts. Leucosome-hosted monazites are characterised by being longer and having a wider range of crystal sizes than those from orthogneiss (protoliths) or from residuum-rich migmatites (i.e., melanosomes) (Fig. 3). This pattern is also observed in the size distribution of zircon (Fig. 4) and has been attributed to grain coarsening via Ostwald ripening (Nemchin et al., 2001). Although the crystal size distribution estimated in this work is based on measured maximum length in thin sections, which underestimates the real greatest radius of the crystal, for comparison purposes it may be considered as a good estimate.

Monazites in melt-rich migmatites show more complex concentric or patchy zoning than those in their protoliths (orthogneisses) (Fig. 1A–C). Larger crystals with more euhedral shape and complex zoning appear in melt-rich migmatites (i.e., leucosomes) than in the residual fractions (Fig. 3). Growth of monazite is suggested during the migmatization event. Three textural types of monazites can be distinguished (Table 2): (i) type-I, unzoned equant grains of small size, (ii) type-II, equant grains with simple and regular (idiomorphic) zoning, and (iii) type-III, more irregular grains with a more diffuse and complex zoning, sometimes concentric or patchy. Occasionally, some type-III monazites in restite-rich granitoids (Fig. 1A,C) show corroded cores with reaction rims, but truncation of zoning or cuspate boundaries have not

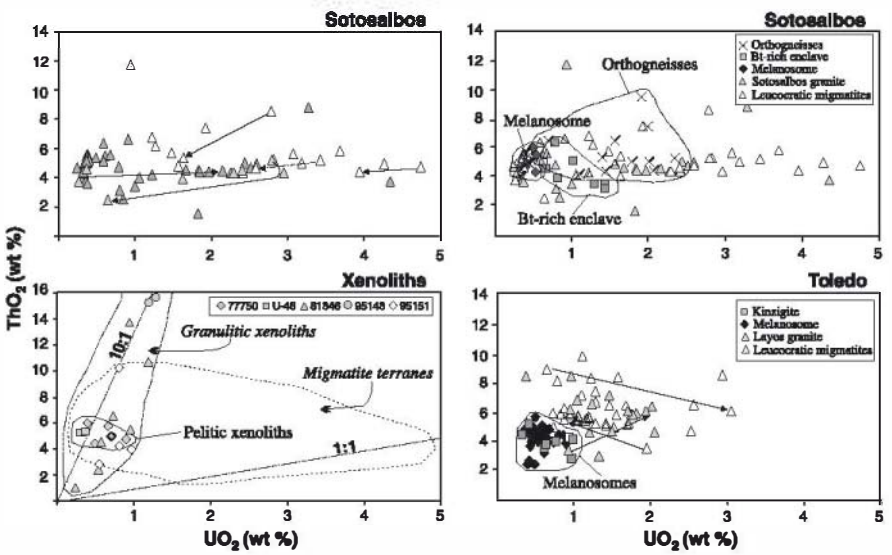

Fig. 5. UO_2 and ThO_2 variation in monatize. Compositional fields of residuum-rich migmatites (melanosomes, bt-rich enclaves) are depicted. Chemical zoning is also marked by arrows from core to rim compositions (see data from Table 3). In the plot of xenoliths, the compositional field of monazite from outcropping migmatite terranes is also shown for comparison.

been observed in any monazite, as occurs in other granulite terranes (e.g. Zhu and O'Nions, 1999).

Type-I monazites are typical of orthogneisses from Guadarrama, but also appear in different granulitic samples together with type-III grains, which are the most common type (Table 2). These two monazite varieties are also found in granulite xenoliths. Type-II monazites with regular zoning have only been found in the Sotosalbos granitoid.

5.3. Xenotime

Xenotime is the least abundant of the studied accessory minerals. It does not appear in the granulitic xenoliths and is very scarce in the granulitic migmatites (Table 1). Hence, its modal abundance decreases rapidly with increasing metamorphic grade until total consumption, as occurs in other crustal sections with peraluminous lithologies (Bea and Montero, 1999; Pyle and Spear, 1999). It appears as equant grains, variably corroded and locally associated with apatite or zircon grains (Fig. 1E). Xenotime crystal size rarely exceeds 50 μm in diameter (Fig. 2). Sieved textures have been observed, constituted by inclusions of major minerals. Two types of xenotime crystals are observed: (i) unzoned or (ii) with patchy or regular concentric zoning. This latter type usually appears in Sotosalbos leucosomes (Fig. 1D).

5.4. Zircon

Modal proportions of zircon decrease from granulitic terrane samples to the xenolith suite (Fig. 2). A slight increase in zircon length is observed between melt-rich and residuum-rich migmatites (Fig. 3), similar to the monazite size distribution. This zircon

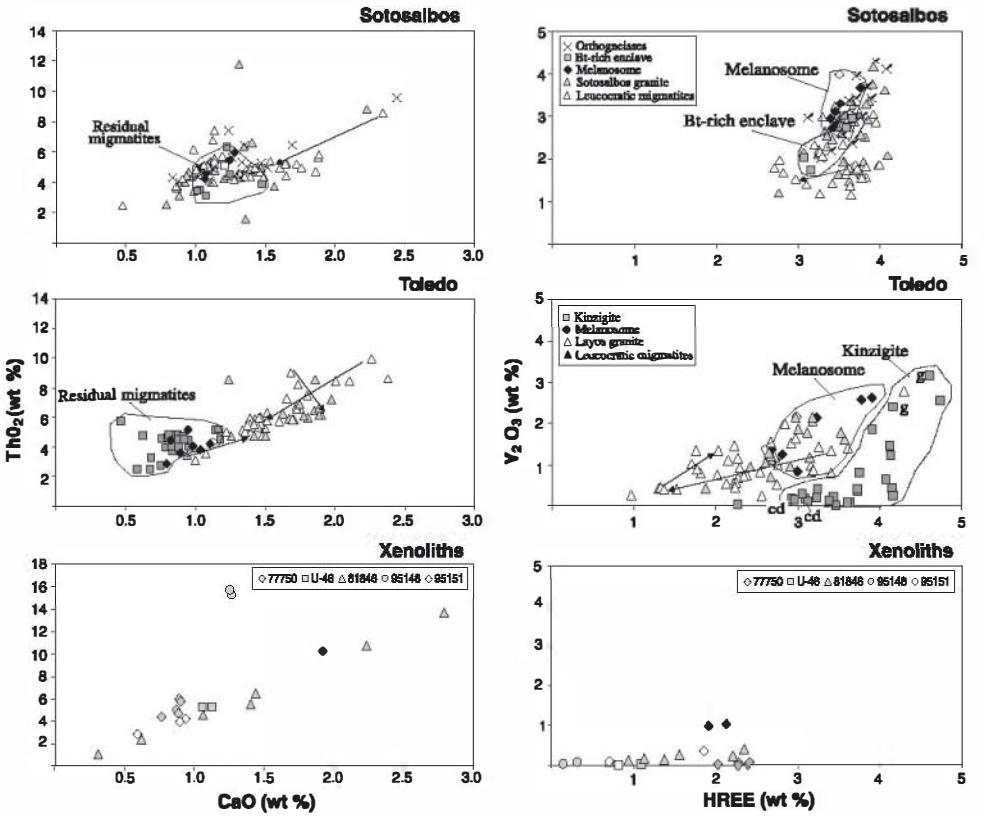

Fig. 6. CaO vs. ThO_2 and HREE vs. Y_2O_3 variation in monazite. Monazites included in garnet (gt) or in their cordierite aureole (crd) from kinzigite sample are marked (see data from Table 3). Same symbols as in Fig. 5.

Table 4
Representative EMP analyses of xenotimes

Sample	Anal			Ce_2O_3	Pr_2O_3	Nd_2O_3	Sm_2O_3	Gd_2O_3	Tb_2O_3	Dy_2O_3	Ho_2O_3	Er_2O_3	Yb_2O_3	Lu_2O_3	Y_2O_3	ThO_2	UO_2	SiO_2	CaO	P_2O_5	Total
Sotosalbos Complex																					
60870	Orthogneiss	3	1	0.34	0.06	0.54	0.15	1.85	1.20	4.69	0.86	4.52	3.87	0.94	43.01	0.44	0.82	0.25	0.05	34.71	98.30
60870	Orthogneiss	4	c	0.32	0.06	0.50	0.21	1.91	1.24	4.78	0.91	4.40	3.58	0.94	43.16	0.46	0.62	0.22	0.06	34.43	97.79
60870	Orthogneiss	5	c	0.35	0.06	0.50	0.20	1.90	1.17	4.75	0.87	4.56	3.84	0.95	43.06	0.21	0.69	0.14	0.10	35.52	99.21
100945	Orthogneiss	13	dz	0.19	0.06	0.30	0.04	1.50	1.48	4.39	1.06	4.81	4.54	1.07	41.74	0.15	1.42	0.33	0.03	33.92	97.42
100945	Orthogneiss	14	bz	0.25	0.06	0.30	0.12	1.62	1.48	4.38	1.02	4.52	4.35	1.00	41.02	0.47	3.57	0.72	0.07	34.30	99.69
100560	Granite	3	unz	0.23	0.00	0.32	0.00	1.77	1.39	4.83	1.07	4.49	4.28	1.08	42.14	0.06	1.02	0.16	0.07	35.21	98.47
100560	Granite	4	unz	0.31	0.03	0.52	0.18	1.86	1.52	4.91	1.16	4.54	4.15	1.01	42.43	0.31	0.69	0.23	0.07	34.68	98.98
101638	Leucosome	27	c	0.26	0.05	0.28	0.11	1.69	2.92	4.26	0.76	3.43	3.47	1.49	42.39	0.20	2.83	0.41	0.37	33.44	98.75
101638	Leucosome	28	r	0.26	0.00	0.32	0.12	1.80	2.88	4.70	0.80	3.40	3.47	1.58	41.70	0.06	1.55	0.20	0.14	33.64	96.95
102183	Leucogranite	28	dz	0.22	0.01	0.26	0.15	1.94	2.95	4.03	0.66	3.68	3.09	1.69	43.04	0.04	1.54	0.27	0.14	33.99	98.12
102183	Leucogranite	27	dz	0.20	0.02	0.26	0.11	2.10	2.84	4.00	0.67	3.67	2.91	1.67	41.86	0.08	2.55	0.35	0.17	33.40	97.26
102183	Leucogranite	26	bz	0.27	0.04	0.35	0.14	1.88	2.72	3.84	0.62	3.48	2.86	1.54	40.34	0.39	6.43	0.99	0.27	32.07	98.80
102183	Leucogranite	35	r	0.23	0.02	0.34	0.19	2.03	2.62	4.27	0.66	3.66	3.07	1.59	42.70	0.08	2.51	0.42	0.16	33.22	98.17
102183	Leucogranite	33	c	0.36	0.09	0.59	0.28	2.00	2.62	4.03	0.63	3.51	3.00	1.46	40.88	0.50	4.29	0.89	0.24	32.90	98.75
100562	Bt-enclave	1	unz	0.22	0.01	0.32	0.05	1.91	0.99	4.79	0.93	4.07	4.26	1.16	42.25	0.03	1.46	1.31	0.12	34.00	98.23
100562	Bt-enclave	2	unz	0.22	0.00	0.38	0.06	2.05	1.09	4.99	0.96	4.21	4.72	1.27	42.30	0.00	1.38	0.15	0.13	35.79	100.12
Toledo Complex																					
93193	Layos granite	1	unz	0.30	0.08	0.50	0.19	1.70	1.05	4.33	0.95	4.53	4.81	1.07	42.90	0.11	1.16	0.17	0.22	35.94	100.47
93193	Layos granite	16	unz	0.30	0.00	0.50	0.20	1.83	1.13	4.71	1.07	4.33	4.62	1.11	41.36	0.03	0.86	0.29	0.24	32.98	96.02

r = rim, c = core, i = intermediate zone, unz = unzoned crystal, dz = dark zone, bz = bright zone.

coarsening in melt-rich migmatites has been also observed in other migmatite terranes (Tanner and Behrmann, 1997; Nemchin et al., 2001).

The scarcity of *igneous* A-type zircons (after Watt et al., 1996), with complex and concentrically regular zoning, in the studied granulitic samples is remarkable. Nevertheless, A-type zircons (>100 μm) with aspect ratios >2.0 and oscillatory zoning (without truncations or overgrowths) have been found in melt-rich migmatites (Fig. 1G), and rarely in xenoliths (Table 2). Granulitic samples usually have more irregular grains of the other three more common zircon-types. These are: (i) irregular grains with corroded core-zoning, usually truncated by unzoned rims (type-B of Watt et al., 1996) (Fig. 1H); (ii) equant grains with minor vague zoning, sometimes truncated by the corroded edge of the crystal (type-C of Watt et al., 1996); and (iii) unzoned small zircon crystals (type-D) (Fig. 1F). These three types appear in xenoliths and migmatite varieties (Table 2), although some leucosomes are very poor in accessory phases (Table 1, Fig. 2). The three types have a similar equant, usually corroded shape, rarely exceeding 100 μm in size.

Although zoned zircons with residual cores surrounded by overgrowth rims (A- and B-types) are not abundant in melt-poor migmatites (e.g. melanosomes, biotite-rich xenoliths), their presence suggests exposure or interaction with a melt fraction (Watson, 1996), even when the zircon is hosted in biotite.

Zircons rarely contain inclusions, although in certain cases rounded inclusions of most of the rock major minerals, particularly those involved in biotite-breakdown reactions have been observed. Sillimanite inclusions are common in samples from lower crustal xenoliths (Fig. 1F), but inclusions of quartz, biotite, sillimanite, plagioclase, and also apatite are observed in other samples (Table 2). As with monazite, zircon may display rims of sieved appearance, or be interstitial to other major minerals.

6. Variations in chemical composition of the accessory assemblages with increasing metamorphic grade

Monazite shows variations in Th, U, Y and HREE contents with the metamorphic grade similar to other peraluminous granulites (Watt and Harley, 1993; Bea and Montero, 1999). The granulitic xenoliths have monazites rich in Th (up to 15 wt.% in ThO_2), but markedly depleted in Y, HREE and U, in comparison to those monazites from migmatites of granulite terranes (Figs. 5 and 6). As a consequence, monazites of granulitic xenoliths have Th/U ratios in the range of 13–20 (Table 3), very similar to the values found by Bea and Montero (1999) in the deepest crustal granulites of Ivrea-Verbano zone. The opposite chemical trend is shown by pelitic monazites from sectors of increasing metamorphic grade (greenschist to upper amphibolite facies) (Franz et al., 1996; Heinrich et al., 1997).

In residual granulitic xenoliths, monazites are also rich in Ca (Fig. 6), displaying a large range of compositions (up to 2.8 wt.% CaO), even at thin section scale (sample 81846 in Fig. 6). It is remarkable that such high-Ca monazites remain residual in lower crustal levels, as it has been stated that CaO increases monazite solubility in granitic melts (Wolf and London, 1995). The high ASI values of the xenoliths and their corresponding melt counterparts (SCS granites)

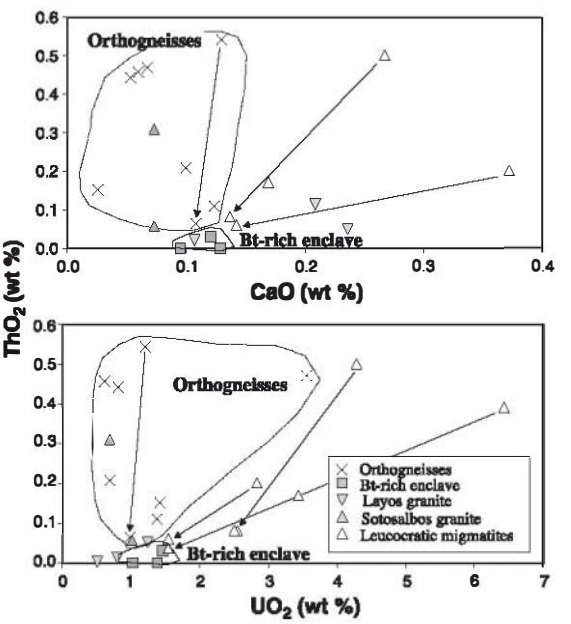

Fig. 7. UO_2, CaO and ThO_2 variation in xenotime. Arrows show the typical zoning of decrease in U, Th and Ca contents in some crystals from leucocratic migmatites of Sotosalbos complex.

Table 5
Representative EMP analyses of zircons

Sample	Anal			Er_2O_3	Yb_2O_3	Lu_2O_3	Y_2O_3	ThO_2	UO_2	ZrO_2	HfO_2	SiO_2	P_2O_5	FeO	Total
Sotosalbos Complex															
100560	Granite	60	c	0.15	0.05	0.00	0.00	0.00	0.00	66.46	0.95	31.07	0.06	0.01	99.00
100560	Granite	61	r	0.21	0.15	0.00	0.22	0.02	0.00	66.52	0.93	30.71	0.34	0.04	99.42
100941	Granite	52	c	0.46	0.57	0.05	2.25	0.14	0.25	64.18	1.12	30.08	1.85	0.28	101.29
100941	Granite	53	r	0.17	0.20	0.05	0.36	0.01	0.03	67.36	1.46	30.87	0.41	0.52	101.46
100563	Granite	34	c	0.14	0.13	0.04	0.17	0.13	0.14	67.54	1.37	31.16	0.04	0.07	101.19
100563	Granite	39	r	0.20	0.22	0.01	0.49	0.02	0.04	67.12	1.67	31.22	0.62	0.02	101.67
100563	Granite	35	r	0.18	0.18	0.02	0.68	0.00	0.00	65.63	1.46	30.78	0.71	0.24	100.11
100563	Granite	36	c	0.52	0.48	0.06	3.56	0.05	0.05	62.05	1.05	28.97	2.93	0.21	100.80
100943	Granite	10	c	0.15	0.19	0.01	0.18	0.04	0.00	66.26	1.05	32.17	0.04	0.01	100.48
100943	Granite	11	r	0.21	0.21	0.05	0.23	0.04	0.36	63.80	2.89	31.59	0.11	0.00	99.88
62458	Orthogneiss	17	i	0.24	0.04	0.00	0.05	0.00	0.00	66.58	1.68	31.61	0.08	0.34	100.86
62458	Orthogneiss	19	c	0.24	0.20	0.01	0.35	0.00	0.03	65.40	1.65	31.30	0.43	0.31	100.11
62458	Orthogneiss	21	c	0.10	0.10	0.01	0.15	0.02	0.00	66.22	1.45	29.86	0.25	0.35	99.04
60870	Orthogneiss	6	i	0.18	0.15	0.05	0.34	0.01	0.01	64.67	1.52	30.70	0.40	0.05	98.30
60870	Orthogneiss	12	r	0.19	0.09	0.01	0.09	0.01	0.00	65.24	1.13	31.59	0.21	0.18	98.99
60870	Orthogneiss	13	c	0.24	0.10	0.04	0.34	0.07	0.14	65.36	0.99	31.72	0.11	0.16	99.55
100945	Orthogneiss	8	dz	0.10	0.15	0.02	0.03	0.01	0.00	67.31	0.83	30.75	0.26	0.15	99.83
100945	Orthogneiss	9	bz	0.09	0.10	0.00	0.13	0.13	0.07	66.59	0.62	30.80	0.09	0.18	99.09
101638	Leucosome	29	c	0.16	0.16	0.01	0.31	0.00	0.02	65.56	1.40	31.46	0.36	0.00	99.64
102178	Leucosome	12	c	0.12	0.04	0.02	0.00	0.01	0.00	66.32	1.25	31.15	0.03	0.02	99.16
102178	Leucosome	13	r	0.22	0.16	0.05	0.17	0.00	0.03	65.14	1.53	31.67	0.26	0.02	99.43
102181	Leucosome	11	unz?	0.08	0.03	0.01	0.00	0.00	0.25	64.28	3.55	31.08	0.05	0.00	99.54
102181	Leucosome	4	c	0.08	0.04	0.00	0.01	0.03	0.00	67.13	1.12	31.58	0.06	0.12	100.45
102181	Leucosome	7	r	0.10	0.14	0.09	0.19	0.02	0.07	65.94	1.62	31.26	0.26	0.17	100.05
100562	Bt-rich enclave	8	c	0.15	0.09	0.01	0.10	0.00	0.00	66.73	0.84	31.11	0.09	0.36	99.72
100562	Bt-rich enclave	9	r	0.13	0.10	0.02	0.08	0.01	0.06	66.11	1.54	29.75	0.22	0.41	98.63
100562	Bt-rich enclave	14	c	0.10	0.11	0.01	0.04	0.11	0.01	66.56	1.68	30.55	0.04	0.42	99.90
102175	Melanosome	1	c	0.05	0.13	0.05	0.28	0.01	0.00	65.53	1.52	31.91	0.35	0.09	100.21
102175	Melanosome	2	r	0.01	0.14	0.04	0.20	0.00	0.07	65.66	1.59	31.26	0.39	0.18	99.75
102175	Melanosome	26	c	0.11	0.11	0.06	0.36	0.04	0.02	65.86	1.15	29.78	0.37	0.20	98.26
102175	Melanosome	27	r	0.10	0.15	0.04	0.39	0.00	0.06	65.93	1.41	29.57	0.44	0.21	98.52
Toledo Complex															
93198	Melanosome	2		0.26	0.05	0.00	0.02	0.02	0.11	66.35	1.14	30.85	0.00	0.07	99.04
93198	Melanosome	3		0.17	0.10	0.00	0.14	0.02	0.05	66.65	0.71	30.46	0.00	0.18	98.90
93198	Melanosome	4		0.14	0.06	0.05	0.05	0.04	0.00	66.71	0.76	30.32	0.00	0.13	98.55
93198	Melanosome	6		0.17	0.10	0.05	0.00	0.15	0.28	66.36	0.82	30.83	0.00	0.12	99.20
81926	Leucogranite	11	c	0.12	0.14	0.04	0.21	0.17	0.16	65.76	0.73	32.30	0.00	0.15	100.20
81926	Leucogranite	13	r	0.34	0.10	0.00	0.06	0.03	0.03	65.67	0.82	32.67	0.00	0.23	100.35
87202	Leucogranite	56	c	0.02	0.06	0.01	0.06	0.01	0.00	65.27	1.25	32.18	0.09	0.02	99.40
87202	Leucogranite	57	i	0.07	0.04	0.00	0.00	0.00	0.18	64.31	1.93	32.05	0.12	0.02	99.08
87202	Leucogranite	58	r	0.23	0.02	0.01	0.00	0.00	0.14	66.10	1.80	32.60	0.09	0.05	101.45
93197	E-leucosome	34	c	0.04	0.20	0.00	0.19	0.01	0.30	64.47	1.40	31.83	0.39	0.11	99.42
93197	E-leucosome	35	r	0.31	0.14	0.01	0.11	0.00	0.53	64.73	1.73	31.96	0.34	0.04	100.40
93197	E-leucosome	44	in-Mon	0.20	0.07	0.03	0.12	0.07	0.23	62.79	1.64	31.29	0.47	0.01	98.16
93193	Layos granite	9	unz	0.25	0.15	0.00	0.53	0.15	0.11	63.05	1.14	31.39	0.69	0.64	98.56
93193	Layos granite	10	c	0.13	0.16	0.01	0.32	0.05	0.00	64.17	1.22	31.64	0.49	0.54	99.02
93193	Layos granite	11	r	0.05	0.07	0.00	0.03	0.03	0.10	61.81	1.59	32.00	0.20	1.29	98.75
93193	Layos granite	15	unz	0.23	0.07	0.00	0.05	0.05	0.01	64.03	1.55	31.64	0.20	0.24	98.29
93193	Layos granite	20	c	0.20	0.24	0.01	0.71	0.20	0.33	62.84	1.25	31.30	0.87	0.38	98.73
93193	Layos granite	27	unz	0.10	0.11	0.03	0.38	0.04	0.10	63.82	1.24	31.53	0.42	0.10	98.59

Table 5 (*continued*)

Sample	Anal			Er_2O_3	Yb_2O_3	Lu_2O_3	Y_2O_3	ThO_2	UO_2	ZrO_2	HfO_2	SiO_2	P_2O_5	FeO	Total
Xenoliths															
77750	Pelitic	2	c	0.15	0.15	0.00	0.00	0.15	0.11	65.12	0.54	33.65	0.77	0.02	101.09
77750	Pelitic	3	i	0.01	0.06	0.00	0.00	0.02	0.12	66.55	0.75	33.49	0.00	0.00	101.19
77750	Pelitic	4	r	0.08	0.03	0.00	0.00	0.00	0.00	65.55	0.72	34.43	0.00	0.01	100.95
95148	Felsic	2	c	0.13	0.10	0.01	0.06	0.05	0.15	65.58	1.77	32.52	0.11	0.13	100.49
95148	Felsic	3	r	0.13	0.07	0.04	0.00	0.03	0.01	66.98	1.30	33.02	0.06	0.24	101.67
95148	Felsic	7	r	0.13	0.06	0.00	0.00	0.01	0.00	66.31	1.45	31.98	0.10	0.06	100.24
95148	Felsic	8	c	0.14	0.08	0.01	0.12	0.01	0.23	66.09	1.67	31.17	0.21	0.04	99.95
95151	Felsic	11	c	0.19	0.21	0.04	0.67	0.14	0.13	65.88	0.83	30.32	0.34	0.20	99.32
95151	Felsic	12	r	0.09	0.05	0.00	0.00	0.00	0.03	65.81	1.34	30.71	0.03	0.31	98.68
95151	Felsic	14	c	0.13	0.08	0.04	0.27	0.02	0.00	66.05	0.76	30.32	0.05	0.15	98.19
95151	Felsic	15	r	0.10	0.06	0.00	0.00	0.00	0.01	66.87	1.34	30.94	0.10	0.18	100.01
81846	Felsic	22		0.14	0.06	0.02	0.12	0.04	0.05	66.10	1.08	31.04	0.17	0.29	99.35
81846	Felsic	23		0.04	0.04	0.01	0.02	0.01	0.15	66.47	1.38	31.25	0.04	0.69	100.37
81846	Felsic	25	unz	0.20	0.15	0.03	0.49	0.15	0.36	64.78	1.32	30.26	0.40	0.00	98.38
99185	Felsic	20	unz	0.20	0.21	0.06	0.42	0.06	0.29	64.76	1.23	30.66	0.41	0.58	99.80

r = rim, c = core, i = intermediate zone, unz = unzoned crystal, dz = dark zone, bz = bright zone, in-Mon = included in monazite.

could explain in part the incomplete dissolution of monazites during melting events (Montel, 1993).

Monazites in leucosomes of both migmatite terranes (Sotosalbos and Toledo) show a similar trend towards lower Y (and HREE) contents, and higher Th and Ca contents, than in their corresponding melanosomes, but the total variation range is more restricted (Fig. 6). It is also remarkable that some monazite cores in the leucosomes are richer in Th–Ca–U than their rims; this is a reverse zoning compared to that observed in other migmatite terranes, where normal zoning is interpreted as residual cores with magmatic rims (Watt and Harley, 1993). These cores (or intermediate zones when oscillatory zoning is present, 93197 no. 46-47-48, Table 3) cannot be interpreted as residual monazites as residuum-rich migmatites and metamorphic wall-rocks do not have monazites with high Ca, U and Th contents (Figs. 5 and 6). We suggest that the scarce monazite that appears in leucosomes and leucogranites is essentially new. This kind of zoning is sometimes coupled with increasing Y (and HREE) towards the rim. It seems that the newly grown monazite rims tend to converge with monazite compositions from the residuum-rich counterparts.

In melt-rich migmatites and leucogranites, monazites have higher U contents than their residual counterparts (melanosomes, protoliths). Th/U ratios have the lowest values in some leucosomes, approx. 1 (Table 3). Monazites in leucosomes commonly show a marked zonation of decreasing U contents from core to rim (Fig. 5 for Sotosalbos). The ACT melt-rich migmatites show a more heterogeneous population of monazites, i.e., monazites with the U impoverishment trend coexisting with monazites showing a reverse or oscillatory zoning. The same is found with respect to Th–Ca behaviour.

In restite-rich anatectic granitoids (Layos or Sotosalbos types), it is also possible to find a similar heterogeneous chemical population of monazites, either unzoned or with reverse or correlative Th–Ca and Th–U zonings. Some monazite cores are chemically similar to those of the melanosomes suggesting a restitic origin (Fig. 5).

In metapelitic granulites (kinzigite 87085 from ACT), some monazites inside garnet are clearly richer in Y-HREE than those of the cordierite-rich aureole around it (Fig. 6 and Table 3) or elsewhere in the matrix. This chemical equilibrium between garnet and monazite has been observed elsewhere (e.g. Pyle et al., 2001).

Xenotime shows also an enrichment in U and Ca contents in melt-rich migmatites (e.g. leucosomes, Table 4) in comparison to residual migmatites, i.e., xenotimes reach UO_2 contents up to 6.5 wt.% in leucosomes whereas those from residuum-rich migmatites have <1.7 wt.% of UO_2 (Table 4). This leads to a change in their Th/U ratios from an averaged value of 0.5 (cores of xenotimes in orthogneisses) to values as low as 0.03 in leucosomes (Table 4) (Fig. 7).

This enrichment in U contents of xenotimes from leucosomes correlates with that shown by monazites from the same samples, and is also coupled with Ca enrichment. In fact, the zoning in xenotimes from melt-rich migmatites is similar to that in monazites, i.e., there is a marked decrease in U and Ca contents from core to rim (Fig. 7). Xenotimes from orthogneisses also show a zonation of decreasing Th contents but not to such an extent in Ca and U contents. Xenotimes of the Sotosalbos granite plot in the same chemical fields as those from orthogneisses (Fig. 7).

Zircon chemical variability is more restricted (Table 5). The lack of variation in REE–Th–U–Y composition of zircon in plutonic rocks has been also addressed (Hoskin et al., 2000), although minor differences have been used in sedimentary rocks to dis-

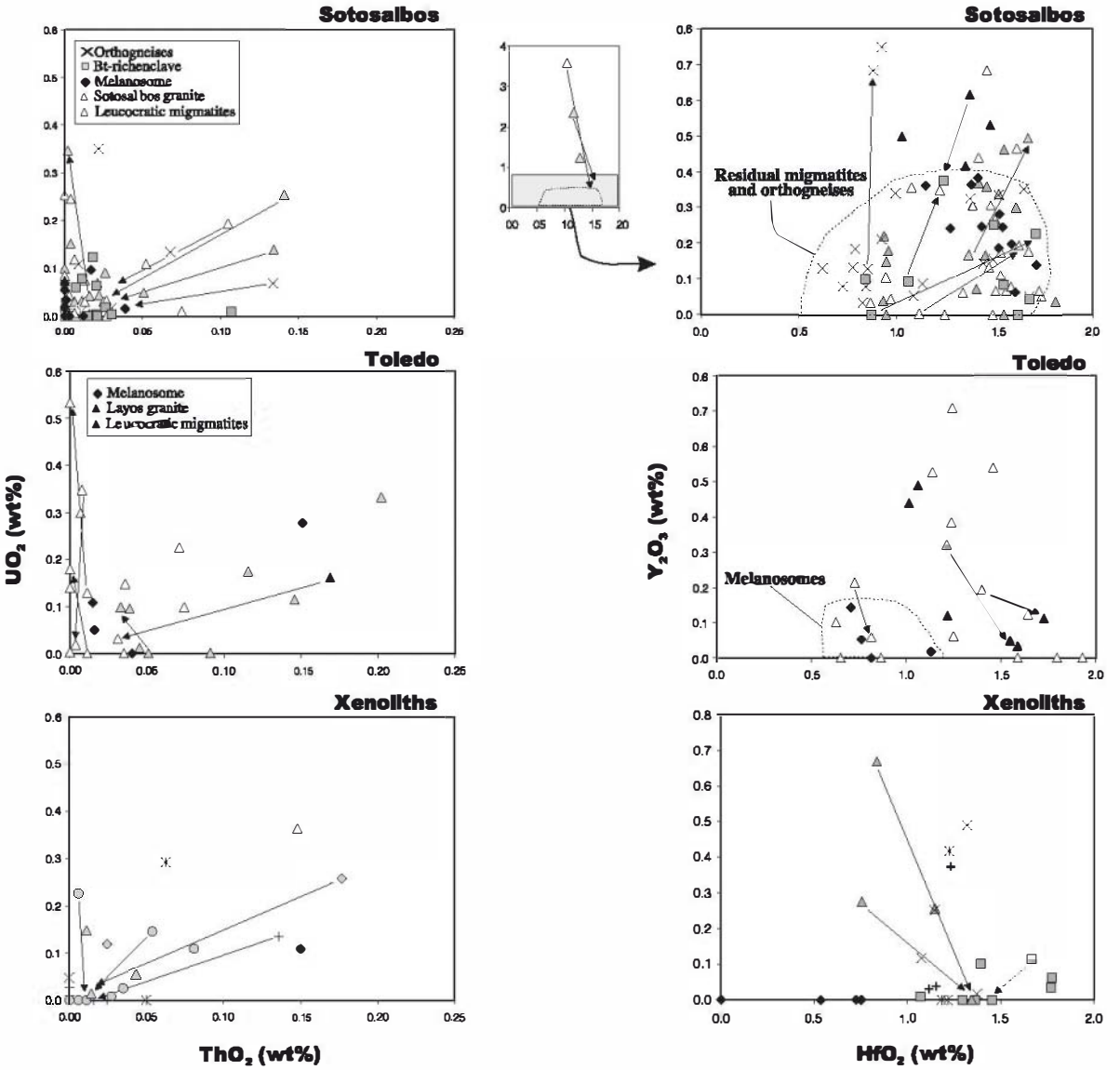

Fig. 8. ThO_2 vs. UO_2 and variation in zircon. Inset in HfO_2–Y_2O_3 plot from Sotosalbos complex showing zircons with residual high-Th cores in anatectic granites. Chemical zoning (core–rim) is shown by arrows.

criminate source regions (Hoskin and Ireland, 2000). The low LREE–MREE–Th–U contents in zircons (qualitatively determined by EMP techniques) make the estimation of trace element differences in zircon chemistry in granulites difficult, although such differences have been suggested by recent studies (e.g. Rubbatto, 2002). Zircons show the same slight zoning from cores rich in Th–U- (Y–HREE–P) towards rims with lower abundances in most of the sampled granulites (Fig. 8). Nevertheless, some low-Th zircons from leucosomes from both migmatite terranes (usually A-type zircons) show the opposite trend to U-rich rims (Fig. 8). It is difficult to interpret the high-Y (and HREE) content in some zircon cores from melt-rich migmatites (usually B-type zircons) as being residual cores, because zircon cores in wall-rock protoliths (and those from residual migmatites) do not show such high Y contents (Fig. 8).

Y and Hf are usually anticorrelated as zircon displays zonations to Hf-rich rims. Nevertheless, when zircon cores are poor in Y (<0.2 wt.% Y_2O_3), the opposite sense of zoning with Y- (and Hf-) rich rims

Table 6
Major (wt.%, EMP analyses) and trace element composition (ppm, LA-ICP-MS analyses) of garnets and feldspar from granulites

	Grt-93198	Grt-93198	Kfs-93198	Grt-99185	Pl-99185	Kfs-99185	Grt-77750	Kfs-77750
n	8	1	2	9	2	1	5	2
		rim						
SiO_2	37.53	37.44	65.35	39.02	61.32	63.63	38.13	64.55
TiO_2	0.05	0.08	0.02	0.11	0.09	0.03	0.12	0.07
Al_2O_3	21.77	21.53	19.44	22.73	24.08	20.35	22.01	19.57
FeO	33.42	34.37	0.11	24.97	0.09	0.03	30.06	0.06
MgO	5.40	4.59	0.01	11.57	0.01	0.00	8.22	0.01
MnO	0.77	1.01	0.01	0.43	0.01	0.00	0.34	0.08
CaO	1.04	1.00	0.09	1.25	5.01	1.49	1.30	0.54
Na_2O	0.09	–	2.63	0.01	7.21	3.9	–	2.84
K_2O	–	–	12.52	–	2.48	9.75	–	11.39
P_2O_5	nd	nd	0.18	nd	0.18	0.18	nd	0.22
Total	99.93	99.94	100.17	99.99	100.21	99.15	100.07	99.02
V	551.5	560.2	2.00	929.9	2.0	2.5	481.2	6.4
Cr	727.3	972.6	3.4	772.8	3.8	3.7	939.3	5.8
Ni	6.6	5.7	3.2	9.5	0.9	1.3	54.3	1.3
Rb	4.6	1.8	335.5	4.4	83.7	60.8	23.9	297.5
Sr	3.4	3.1	379.7	11.6	784.3	635.2	2.7	426.4
Y	751.4	639.0	2.0	652.8	1.8	5.5	563.1	1.4
Zr	140.4	206.3	4.24	492.3	32.4	42.1	439.7	38.9
Ba	8.8	1.8	1661.5	35.8	2358.0	1795.8	9.0	2026.3
La	1.28	0.85	4.87	2.54	228.78	116.90	0.61	88.38
Ce	3.62	1.12	8.38	17.50	541.48	177.19	3.64	185.46
Nd	3.13	1.10	2.19	14.75	57.99	53.38	14.60	5.95
Sm	6.22	5.44	0.24	30.95	5.20	5.84	49.42	1.17
Eu	0.61	0.06	2.69	0.59	5.02	5.52	1.58	4.23
Gd	48.57	50.93	0.72	75.57	2.10	2.19	84.00	0.43
Dy	118.04	102.75	0.19	104.35	0.22	0.66	100.22	0.13
Yb	50.72	20.86	0.24	80.28	0.22	0.39	53.89	0.21
Lu	6.99	1.86	0.08	11.23	0.02	0.15	7.99	0.01
Hf	3.16	5.86	1.07	10.39	1.11	1.49	8.34	0.64
Pb	2.62	2.19	76.16	3.77	37.10	23.85	1.62	30.52
Th	0.92	0.34	0.92	0.55	0.30	0.64	0.05	0.28
U	0.43	0.12	0.20	0.53	0.33	0.51	0.49	0.11
LREE t	14.25	8.51	15.68	65.74	833.44	353.30	68.26	280.97
REE t	239.17	184.97	19.59	337.77	841.02	362.21	315.94	285.97

appears. This reverse zoning is also common in zircons from orthogneisses and residuum-rich migmatites of the Sotosalbos area.

In granulitic xenoliths, zircons show a marked zoning towards rims which are extremely depleted in Y–HREE–Th–U contents (Fig. 8 and Table 5), as has been observed in zircons from other lower crustal xenoliths (Hanchar and Rudnick, 1995).

7. Variations in trace element composition of some major minerals of the granulitic assemblage

Garnets in granulitic xenoliths belong to the almandine-pyrope series (approx. $Alm_{45-50}Pyr_{45-55}$, with slightly more Fe-rich garnets present in pelitic xenoliths: $Alm_{60}Pyr_{35}$) with compositional zoning almost absent in garnet cores (Villaseca et al., 1999). This is not the case for migmatite samples from Toledo Complex which have garnets with pronounced reverse zoning (Barbero, 1995) and are pyrope-poor in composition, indicating shallower equilibration depths. Moreover, there is a slight chemical difference between garnets in leucosomes ($Alm_{75-81}Pyr_{14-21}Sps_{2-7}Grs_{2-4}$) and those of melanosomes ($Alm_{80-88}Pyr_{8-21}Sps_{1-3}Grs_{2-3}$) in the ACT (Barbero, 1995).

Plagioclases in all granulite types are mostly in the range of An_{21} to An_{35}, but those from granulitic xenoliths lack albite-rich rims and have a notably higher Or-component (in the range 10–23 mol% instead of <5 mol% in granulite terranes), indicative of a higher temperature of equilibration (Villaseca et al., 1999). K-feldspars in all granulite types are mostly in the range Or_{70} to Or_{90} showing a high An-content (up to 10 mol%) in those from granulitic xenoliths (always <1 mol% in migmatitic terranes). Feldspars from granulitic xenoliths also show a slightly higher P_2O_5 content, never <0.14 wt.%, i.e., a 20–30% greater than in feldspars from migmatite terranes (Table 6).

ACT mesosome–leucosome pairs have plagioclases with An contents mostly in the range of An_{28}–An_{35} whereas related anatectic granites (Cervatos leucogranites and Layos granitoids) have plagioclases with An_{12} to An_{30} compositions. In Sotosalbos area, the cordierite-bearing granite have feldspars with a slightly higher P_2O_5 contents (average 0.12 wt.% in plagioclase and 0.18 wt.% in K-feldspar) than in related metamorphic country rocks (0.12 and 0.13 wt.%, respectively), as occurs in other granulite terranes (Pan et al., 1999).

Table 6 lists trace-element contents of some major minerals in the granulite assemblages: garnet, plagioclase and K-feldspar, whereas REE patterns for the various minerals analyzed are given in Fig. 9.

Chondrite-normalized REE patterns of the analyzed garnets (Fig. 9) exhibit a marked Eu negative anomaly (up to 0.015) and an almost flat HREE pattern. The general REE-patterns of these minerals are similar to those found by Reid (1990) in lower crustal peraluminous granulites, but markedly different to those found in garnets from mafic granulitic xenoliths (Loock et al., 1990). The flat HREE pattern of the garnets is consistent with their lower crustal

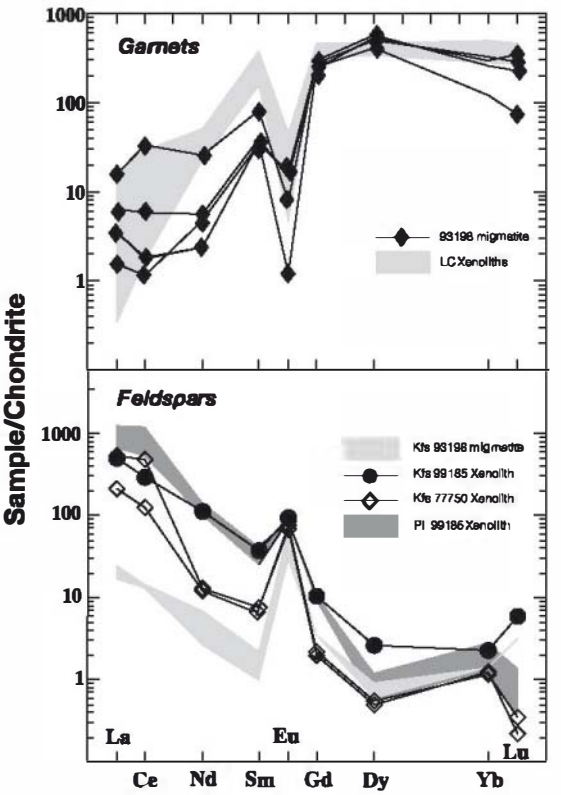

Fig. 9. Chondrite normalized REE patterns of garnets and feldspars. Note progressive increase in MREE in garnets with increasing metamorphic grade. The increase in LREE in K-feldspars from xenoliths is also evident.

derivation as the increase in the Gd/Dy ratio seems to be controlled by load pressure (Bea et al., 1997). It is interesting to note that analyzed garnets have LREE contents higher than chondrite levels, also in agreement with the scarce previous data on felsic granulitic xenoliths (Reid, 1990). Garnets from peraluminous granulites of migmatitic terranes have much lower REE contents (see also Bea et al., 1994, 1999; Harris et al., 1992; Watt and Harley, 1993), in the range of 50–250 ppm whereas granulitic xenoliths have a range of 300–400 ppm (Table 6). Other trace elements greatly concentrated in these granulitic garnets are Y (usually in the range of 550–750 ppm) and Zr (up to 500 ppm). The high Zr contents of these garnets are one order of magnitude greater than the previous published data (Fraser et al., 1997). Nevertheless, some of these high trace elements contents in garnet may be spurious as very small accessories (<2 μm) are difficult to detect in the thick sections used in LA-ICP-MS measurement.

Trace element zoning in analyzed garnets is minimal in comparison to other garnets from granulite terranes from which well defined bell-shaped zoning (Otamendi et al., 2002) or inverse zoning (Bea et al., 1994) have been described. This is in agreement with the decrease in trace element zoning in garnets at higher metamorphic grade observed by Schwandt et al. (1996).

Chondrite-normalized REE patterns of feldspars show great LREE enrichment (sometimes close to × 1000 the chondritic values), with (La/Yb)n ratios as high as 411 being similar in both alkali-feldspar and plagioclase (Fig. 9). Plagioclases have higher La and Ce contents than K-feldspars but similar Eu and HREE contents. The maximum positive Eu anomaly (up to 31) is found in a K-feldspar crystal (granulite 77750). LREE contents of feldspars in granulitic xenoliths range from around 835 ppm in plagioclase to 280–360 ppm in K-feldspar (Table 6). Such a high LREE content of feldspars has never being previously reported in granulitic rocks (Pride and Muecke, 1981; Reid, 1990; Watt and Harley, 1993; Bea et al., 1994; Bea and Montero, 1999) (Fig. 10). The LREE contents of feldspars in granulites from migmatite terranes are markedly lower (Fig. 10). LREE data from feldspars from the two migmatitic terranes of central Spain show contents in the range of around 25–5 ppm (plagioclase and K-feldspar from the Peña Negra

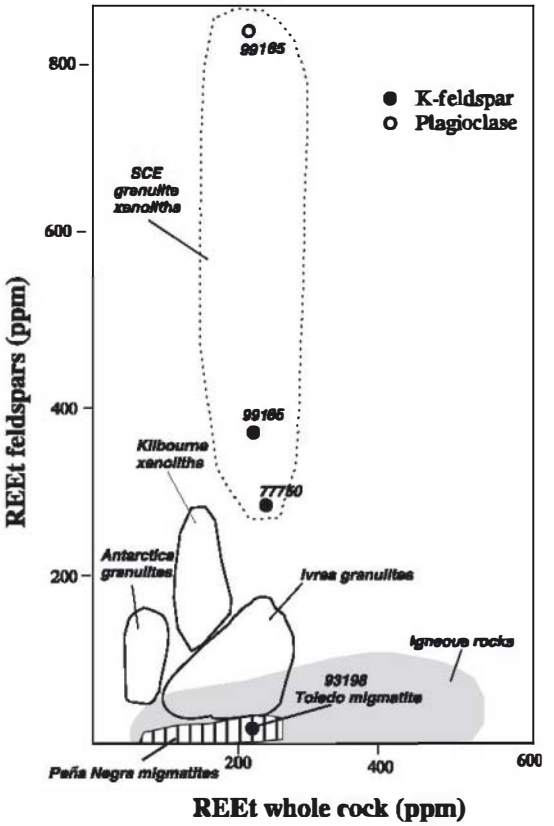

Fig. 10. Comparison of total REE in feldspars and whole rock granulites from migmatite terranes and xenolith suites. Feldspar composition from Toledo migmatite (melanosome 93198) and xenoliths (77750 and 99185) are taken from Table 6. Data from xenoliths are those of Kilbourne Hole (Reid, 1990). Data from migmatite terranes are: Peña Negra (Bea et al., 1994), Ivrea-Verbano (Bea and Montero, 1999) and E-Antarctic Shield (Watt and Harley, 1993). Compositional field of feldspars from felsic igneous rocks is taken from Reid (1990).

complex, Bea et al., 1994) or 16 ppm (K-feldspar from the ACT, Table 6).

8. Discussion

8.1. Trace element residence sites in granulites

The trace element contents of major minerals and their modal proportions can be used to calculate whole-rock compositions for comparison with the whole-rock analyses, in order to evaluate by mass balance the

proportion of elements that reside in major minerals. Whole-rock analyses are listed in Appendix B.

The 93198 melanosome from ACT has REE–Th–Y–Zr trace element bulk-rock contents that are mainly explained by their accessory mineral assemblage, as is usual in igneous and most metamorphic rocks. The major minerals in this sample (modal composition in Table 1) do not have appreciable contents of these elements, totalling < 5% of the LREE–Th–Zr whole-rock concentration (Fig. 11). Most of the LREE–MREE–Th–U in the granulite whole-rock are contained in monazite (and also REE in apatites, Bea et al., 1994), and correlatively, Zr in zircon and Y-HREE in xenotime. This data is in agreement with previous reports in the nearby Peña Negra complex (Bea et al., 1994), where is also shown that biotite or cordierite have even lower REE contents than feldspars. Nevertheless, some exceptions to this are shown in Fig. 11. Garnet is an important host of Y in migmatitic granulites and feldspars have high P contents, too.

In lower crustal granulitic xenoliths, trace element distribution is clearly different. In samples 77750 and 99185 (see modes in Table 1), the major minerals are the host of an important fraction of the REE–Y–Zr of the granulites. The higher LREE contents of their feldspars significantly contribute to the LREE (and also P, Rb, Sr, Ba) contents of the xenoliths, whereas garnet is the main host of Y–HREE and a substantial part of the Zr whole-rock content (Fig. 11). The very high Zr content of the garnets could explain up to the 50% of the Zr in one sample (Fig. 11).

Although some difficulties arise when using modal approaches, and sometimes there are sums >100% (e.g. xenolith 77750 with 0.30Grt with averaged 54 ppm of Yb contents give 16 ppm in rock, much greater than the analyzed 4.3 ppm of whole-rock content), the general picture is consistent with a higher trace element sequestering by the major phases of the granulites with increasing metamorphic grade, and therefore with a diminished contribution of accessory phases to the trace element budget of the granulites. This is in agreement with the preliminary conclusions of Reid (1990).

8.2. Limited dissolution of accessory minerals in granitic melts

The retention of accessory phases (monazite, xenotime and zircon) in melanosomes during partial melting led to the generation of low-REE–Th–Y–Zr melts with disequilibrium chemistry, as has been described in many migmatite terranes (Watt and Har-

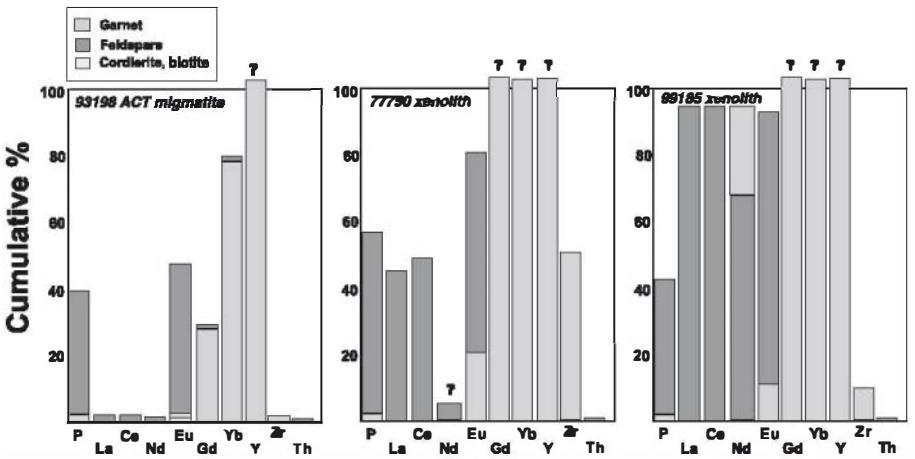

Fig. 11. Relative contributions of the major minerals phases to some trace elements (P–REE–Y–Zr–Th) budgets for some studied granulites. In melanosome 93198 from Toledo complex, trace element contents of cordierite and biotite are taken from those of the nearby Peña Negra complex (Bea et al., 1994). White areas are those trace element contents not explained by major mineral chemistry (i.e., in accessory phases). Note the progressive importance of feldspars and garnet in hosting most of the REE–Y (P–Zr) of the whole rock with increasing metamorphic grade.

ley, 1993; Nabeleck and Glascock, 1995; Johannes et al., 1995), and also in the studied area (Barbero et al., 1995; Villaseca et al., 2001). There is a marked REE fractionation (usually coupled with Zr–Th–Y fractionation) between leucosomes and melanosomes with the two rock types occasionally showing complementary trace element patterns (Fig. 12). The concentration of accessories in the mafic assemblage of the melanosomes (Table 1) could explain this fractionation.

The growth of new monazite, xenotime and zircon in the leucosomes and leucogranites poses the question of the limited dissolution of accessory phases in the melt fraction. Leucosomes in migmatite terranes usually do not represent pure melt fractions (e.g. Johannes et al., 1995; Solar and Brown, 2001). Chemically, the leucosomes present a shift from "experimental minimum" solidus compositions in Qtz–Ab–Or ratios, and their heterogeneous geochemical features suggest the contribution of different processes in leucosome formation: equilibrium/disequilibrium melting, entrainment of residual material, fractionation (including escape of evolved melts) during crystallization, etc. (see review by Solar and Brown, 2001). In any case, leucosomes are (or have been) richer in melt than melanosomes during migmatization. The REE–Th–Y–Zr contents usually displayed by the leucosomes (and associated leucogranites) are lower than those estimated by dissolution models using reasonable temperature values (700 to 800 °C), even using high (4–6 wt.%) water contents in the melt (Barbero et al., 1995; Villaseca et al., 2001). Therefore, only limited dissolution of accessory phases in the melt fraction has occurred. The more enriched-REE varieties of leucosomes (E-types), usually coupled with their higher transition metal contents (Fe, Mg, Ti, Cr, V), have been explained by a higher restitic component (Villaseca et al., 2001).

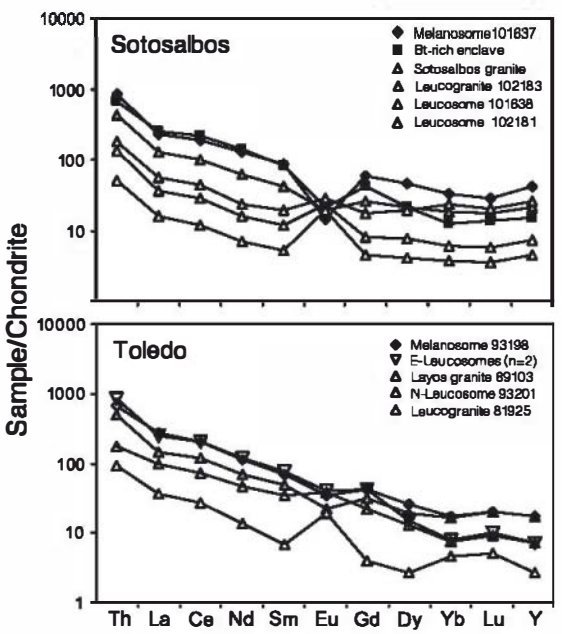

Fig. 12. Chondrite normalized REE patterns for migmatites from the two studied granulite terranes. Note the low REE content and positive Eu anomaly of some leucocratic migmatites of Sotosalbos and Toledo complexes (N-type leucosomes, leucogranites) whereas E-type leucosomes have almost coincident REE patterns than residuum-rich migmatites except by their lower HREE contents. Complementary REE patterns between melanosomes and N-leucosomes are also shown.

An important difference between the two studied migmatite terranes is the fact that the ACT migmatites have been equilibrated under more extreme conditions than those of the Sotosalbos area, as the biotite dehydration reaction has been clearly overstepped close to its total consumption in the ACT (Barbero, 1995). As the biotite is the main host for accessory minerals in peraluminous lithologies, its breakdown liberates inclusions to react and participate in partial melting. In migmatites of the Sotosalbos area, accessories had fewer opportunities to saturate granitic melts, as a substantial amount is armoured in the restitic biotite. No enriched REE–Zr–Th–Y melt-rich migmatites (e.g. E-leucosomes) have been found in Sotosalbos area.

Monazites growing in granitic liquids depleted in LREE will tend to show more ionic substitutions of the kind (e.g. Zhu and O'Nions, 1999):

$$Th^{4+} + Ca^{2+} = 2LREE^{3+} \quad (1)$$

$$U^{4+} + Ca^{2+} = 2LREE^{3+} \quad (2)$$

$$Th^{4+} + Si^{4+} = LREE^{3+} + P^{5+} \quad (3)$$

$$U^{4+} + Si^{4+} = LREE^{3+} + P^{5+} \quad (4)$$

These substitutions are very common in the studied migmatites as illustrated in Fig. 13 where (Th + U) is linearly related to (Si + Ca), suggesting the overall existence of the coupled substitutions (Eqs. (1)–(4)).

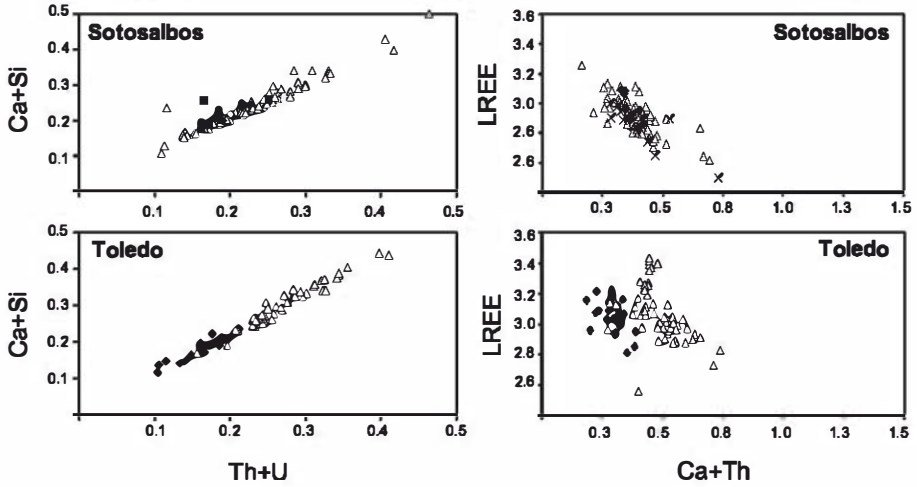

Fig. 13. Plots of (Th + U) vs. (Ca + Si) and (Ca + Th) vs. (LREE = La + Ce + Nd) of monazites from studied migmatites from granulite terranes. All elements are in at.%. Same symbols as in Fig. 5.

Nevertheless, the introduction of Ca is significantly more marked than Si, suggesting a major role of substitutions (1) and (2). Individually, Si does not show any correlation with (Th + U) contents. The introduction of Ca and U in monazites is in agreement with the undersaturation in REE of the melt-rich migmatites. In the more REE-saturated melt-rich migmatites of Toledo (E-leucosomes, E-leucogranites), monazites show cores that are less enriched in U than those of Sotosalbos area (Fig. 5). Moreover, substitutions (1) and (2) are less marked in those samples (Fig. 13).

Peraluminous granites of the SCS batholith are also undersaturated in trace elements. They always have <250 ppm of total REE or Zr, much less than concentrations obtained using reasonable combinations of parameters involved in solubility models of accessory phases (Villaseca and Herreros, 2000). Small accessory grains would be expected to have dissolved if they had been in equilibrium with granitic melts. For instance, most of the small zircons (<120 μm) would be dissolved in granitic melts at high temperature (>850 °C) (Watson, 1996), but they survive in granulitic xenoliths (Fig. 2). Two possibilities arise to explain the low REE–Zr dissolution in the SCS granitic melts: (i) the granulitic xenoliths were not equilibrated with granitic melt, and (ii) if the xenoliths underwent partial melting, the granitic melts were not equilibrated with zircon/monazite dissolution. The granulitic xenoliths have been interpreted as restite materials as they are more mafic than their pelitic or orthogneissic parents as would be expected from a mass balance of partial melting of metasediments (or metaigneous rocks) from which a granite melt was removed (Villaseca et al., 1999). Major and trace element modelling indicates than an average of 30% of peraluminous granitic melt was extracted. The isotopic (Sr, Nd, ●) data are also consistent with the suggested genetic relationship of the granulitic xenoliths being melting residua after the extraction of liquids similar in composition to the SCS granites (Villaseca et al., 1999; Villaseca and Herreros, 2000).

If granulitic xenoliths were the residuum of a melting event, the survival of small zircon and monazite crystals implies a low solubility in the peraluminous granitic melts (second hypothesis). Trace minerals have not been armoured in reactant minerals (most of accessories are in the new granulitic minerals: feldspars or garnets) and they have unequivocally grown during peak metamorphism. As P–T conditions were more extreme than in granulitic terranes and perhaps the thermal event could also have been longer, the more reasonable solution to this limited accessory-phase dissolution in granitic melts might be that they were included in the newly crystallizing

minerals and also by the competition of this new granulitic mineral assemblage (feldspars and garnet) in sequestering trace elements, as will be discussed in more detail below.

8.3. REE–Y–Zr compatible character of feldspars and garnets in extreme granulitic conditions

Sequestering of trace elements by major minerals in peraluminous high-grade granulites has been previously described. Bea and Montero (1999) show an inverse relationship between the modal abundances of xenotime and garnet which, combined with the high HREE–Y contents in garnet, has been interpreted to indicate that xenotime was consumed in garnet-forming reactions. Reid (1990) also found high-LREE feldspars and high-HREE garnets in peraluminous granulites from lower crustal xenoliths. She supposed two alternatives to explain the low activities of accessory minerals in the trace element budget: (i) the stability of a REE-bearing phase(s) may have been exceeded with increasing temperature and was probably related to biotite dehydration reactions, or (ii) the partition coefficients of REE-rich accessory phases would have to decreased differentially with respect to those of the major mineral phases by a factor of at least two. The first factor could be argued for xenotime but not for zircon or monazite which participated continuously in metamorphic reactions in these xenoliths.

Bea et al. (1994) give an estimate of mineral/melt partition coefficients for rock-forming minerals under conditions of mid-crustal anatexis in peraluminous systems (Peña Negra complex). Their data show that feldspars (especially plagioclase) could have high-LREE partition coefficients during granulite-facies conditions, suggesting that LREE become clearly compatible in the feldspar structure. They propose mineral/melt K_d^{REE} values in feldspars (plagioclase and K-feldspar) around 10 times greater than those estimated for felsic granitic magmas (Nash and Crecraft, 1985). With respect to garnet, Bea et al. (1994) also propose much higher HREE–Y partition coefficients than those based on pure magmatic systems. Correlatively, monazite/leucosome ratios are also an order of magnitude higher than those estimated for magmatic systems (Bea et al., 1994). Nevertheless, these high K_d values are consequence of their estimation from simple normalization to their migmatitic component (leucosome) which is severely depleted in REE–Th–Y–Zr contents and assumed to be pure and equilibrated anatectic melts. In fact, the relative mineral/mineral REE-partition coefficient between monazite and feldspars in Peña Negra migmatites does not change significantly when compared to those determined in magmatic systems (Fig. 14). This is not the case for our data on ACT migmatites (Fig. 14). For this comparison, we have calculated mineral/mineral partition coefficients as the average monazite/mineral ratio for each RE element (see also Kretz et al., 1999). The LREE partition coefficients obtained are around the half of those determined in the Peña Negra anatectic complex (Bea et al., 1994) or those obtained from magmatic systems (Bea, 1996) (Fig. 14).

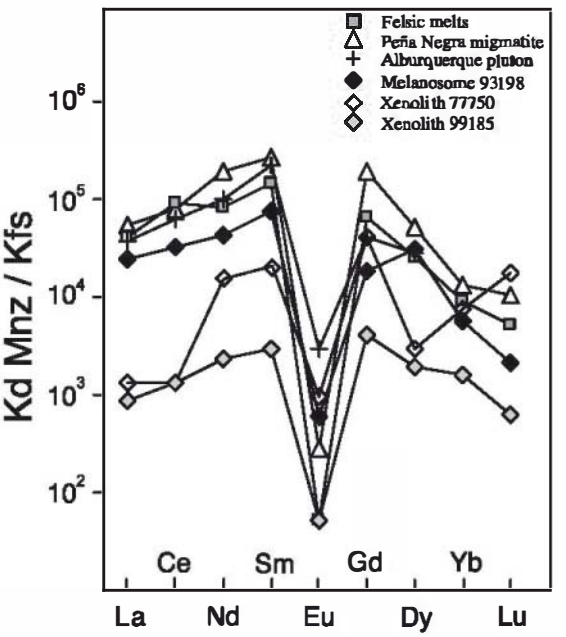

Fig. 14. Monazite–K-feldspar partition coefficient from different granulites and felsic igneous rocks. Individual samples from studied Toledo granulitic terrane and xenolith suite are indicated. Data for felsic melts is calculated by dividing monazite/melt partition coefficient from Yurimoto et al. (1990) by K-feldspar/melt partition coefficient from Nash and Crecraft (1985). Data for Alburquerque granitic pluton are taken from Bea (1996) (monazite analysis 2 from Table 7 and Kfs analysis 2 from Table 4). Data for Peña Negra migmatite are taken from melanosome ms-1 of Bea et al. (1994). Note the progressive lowering of partition coefficients with increasing metamorphic conditions.

Fig. 14 also shows the estimated REE partition coefficients between monazite and K-feldspar in the lower crustal xenoliths. It suggests a significant change in the behaviour of REE between both minerals as a consequence of their progressive chemical change with increasing metamorphic grade. LREE in feldspars become progressively more compatible whereas monazite reduces its activity in controlling REE geochemistry. The reduced activity of accessory phases in controlling trace element geochemistry in lower crustal scenarios cannot be related to their dissolution in the granitic melts generated during the different partial melting events. Their decrease might be related to their partial consumption during participation in dehydration (melting) reactions. As an example, if we use Eq. (3) of Spear and Kohn (1996) to model changes in trace element concentrations in a K-feldspar when monazite is being consumed, we obtain that with just a 0.0005 mol% of consumption of monazite (supposing D^{LREE} monazite-K-feldspar around 30,000 from Tables 3 and 6; whereas a value of 107,000 is obtained from data of Bea et al., 1994) K-feldspar could increase their LREE contents by 15 to 50 times. This is a difference of the same magnitude as we obtain when comparing LREE contents in feldspars from granulite terranes to those of granulitic xenoliths (Table 6).

8.4. Transfers of REE, Th, U, P and Zr among granulitic minerals

Crystallization of monazite and zircon during prograde metamorphism is usually related to the presence of pre-existing accessory minerals (Bingen et al., 1996; Pan, 1997). This is supported not only by textural relationships among accessory minerals but also by the immobile behaviour of many trace elements during metamorphism that would require their transport over short distances. Formation of monazite and zircon from the breakdown or recrystallization of pre-existing REE–P–Th–U–Zr-rich trace minerals requires only very localized remobilization of these trace elements and therefore is favoured (Pan, 1997). The consumption and modal decrease of accessory minerals with increasing metamorphic grade in the studied crustal section is in agreement with this statement. Nevertheless, two situations could be envisaged in our study. In migmatite terranes, the growth and recrystallization of monazite, xenotime and zircon is mainly controlled by the previous accessory assemblage of the rocks (amphibolite to granulite facies transition related to the beginning of the biotite dehydration melting reaction). In lower crustal xenoliths, the exhaustion of accessory minerals is so extensive that the major silicate minerals receive a significant portion of the REE and Zr liberated by their breakdown (metamorphic conditions close to total consumption of biotite, in fact an Al-Ti-rich phlogopite in composition, Villaseca et al., 1999).

In the absence of other REE-rich accessory minerals (e.g. allanite, titanite), recrystallization of monazite in peraluminous granulites is usually ascribed to apatite breakdown as demonstrated both in experiments (Wolf and London, 1995) and in detailed mineral studies (Pan, 1997; Simpson et al., 2000). The positive correlation between the modal decrease of apatite and the major introduction of Ca and U in monazite (substitutions (1) and (2) above) suggests a key role of apatite in transferring not only Ca, U, (Th) but also P and REE to monazite (Fig. 15). The same situation occurs in xenotime,

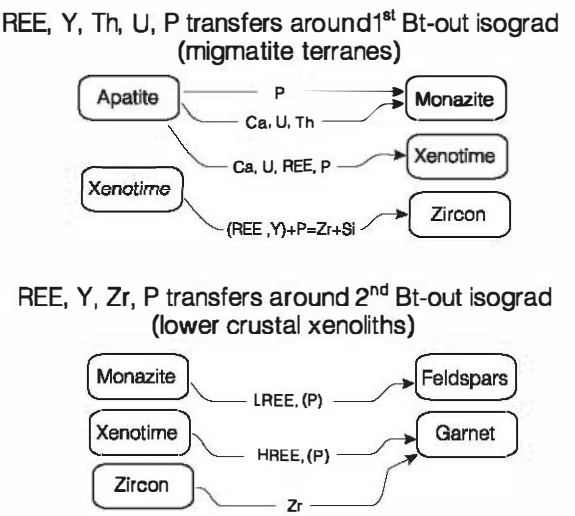

Fig. 15. Schematic transfers of REE, Th, U, P among minerals of migmatites from granulite terranes (breakdown of biotite or first biotite-out isograd) and granulites from xenolith suite (close to Ti-phlogopite-out isograd or second biotite-out isograd).

which also shows a marked increased in Ca and U in its crystal cores (Fig. 7). In both cases, apatite could be involved coupled with the general biotite breakdown reaction:

$$(\underset{\text{in-apatite}}{\text{U, TH, REE}}) + \text{biotite} + \text{plagioclase} + \text{sillimanite} + \text{quartz} \rightarrow (\underset{\text{in-monazite-core}}{\text{Ca, Th, U, LREE}}) + (\underset{\text{in-xenotime-core}}{\text{Ca, U, Th, Y, HREE}}) + \text{K-feldspar} + \text{garnet/cordierite} + \text{melt}$$

The chemical control of monazite when hosted in garnet or cordierite suggests the involvement of these minerals in some trace element transfer.

In the case of zircon, the presence of P–Y–HREE-rich cores suggests the involvement of a phosphate in their formation and/or recrystallization. The contents of Y, Ca and P in these granulitic zircons are greater than those in granitic rocks (Hoskin et al., 2000). A plot of Y+REE (atom) vs. P (atom) reveals that for most granulitic zircons there is a (REE,Y)/P substitution of 1:1 (Fig. 16) suggesting that xenotime is clearly involved in their genesis transferring some HREE–Y–P components (Fig. 15).

The main role of accessory minerals in controlling REE–Y–Th–U–Zr geochemistry of migmatite granulites changes drastically in lower crustal scenarios where accessories are progressively consumed in metamorphic reactions. The total consumption of xenotime, as manifested by its absence in the xenoliths and the high Y (and Zr)–HREE-contents in restitic garnet, suggests the involvement of these accessories (xenotime, zircon) in their formation:

$$\underset{\text{xenotime}}{(\text{Y, HREE})\text{P}\bullet_4} + \underset{\text{zircon}}{(\text{HREE})\text{ZrSi}\bullet_4} + \text{AlTi-phlogopite} + \text{plagioclase} + \text{sillimanite} + \text{quartz} \rightarrow (\underset{\text{in-garnet}}{\text{Y, HREE, Zr}}) + \text{K-feldspar} + \text{melt}$$

Other minerals in the xenoliths (e.g. sillimanite, quartz or rutile) do not show appreciable contents of these trace elements. REE-P-rich feldspars (plagioclase and K-feldspar) are related to monazite and probably apatite breakdown, as their modal decrease in these granulites is very noticeable (Table 1). A general mica consumption reaction with participation of accessories would be as follows:

$$\underset{\text{monazite}}{(\text{LREE})\text{P}\bullet_4} + \text{apatite} + \text{Al-Ti-phlogopite} + \text{plagioclase} + \text{sillimanite} + \text{quartz} \rightarrow \underset{\text{K-feldspar}}{(\text{LREE, Na, K})\text{AlSi}_3\bullet_8} + \text{garnet} + \text{rutile} + \text{melt}$$

the residual plagioclase being also enriched in LREE components (Fig. 15).

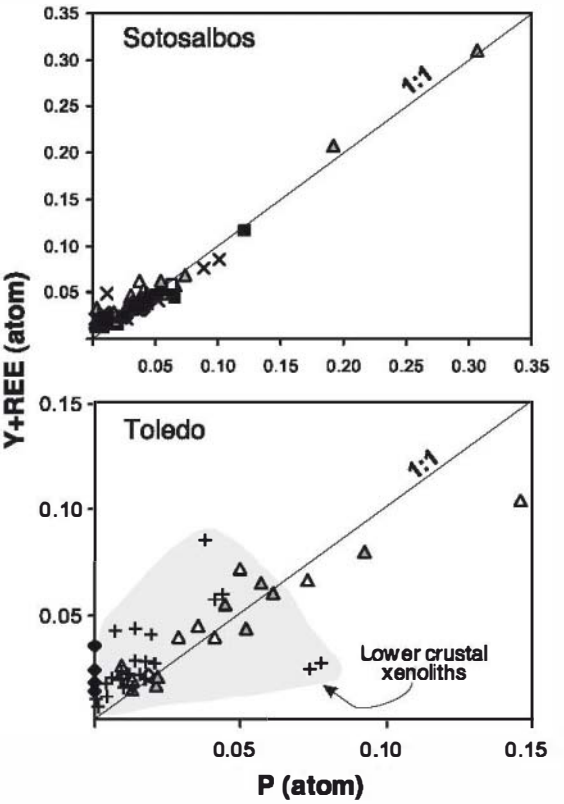

Fig. 16. Plot of Y+REE vs. P of zircons from studied samples. Zircons from lower crustal xenoliths (crosses) are included in the shaded field. A one-to-one ratio of REE to P indicates xenotime substitution. All elements are in at.%. Symbols as in Fig. 5.

9. Conclusions

Although accessory minerals may occur as newly crystallized phases, overgrowths and re-growths during high-grade metamorphism, there is a marked decrease of their modal abundance in lower crustal xenoliths under more extreme granulite facies conditions.

The existence of crystal coarsening, the growth of idiomorphic and sometimes complex oscillatory zoning (e.g. A-type zircons or type-II monazites), and the appearance of new chemical features in monazite and xenotime crystals (zircon remains more constant), lead to the supposition that most accessories in melt-rich migmatites are newly crystallized, in agreement with the data of Nemchin et al. (2001). Therefore, a redistribution of trace elements in the early stages of granulite facies conditions, during biotite-breakdown (first biotite-out isograd), is required. At this stage, most trace elements are hosted in accessories although in most granulitic rocks they are isolated and interstitial, therefore separated by hundreds of microns (much more in the case of accessory-poor lithologies: N-leucosomes or leucogranites). Nevertheless, reactions and chemical transfer between accessory minerals seem to be supported by their chemical variation and substitutions. In some melt-rich migmatites, the presence of low-HREE–Y and high-U–Ca monazite cores (or high-U–Ca xenotime cores) suggests their growth from a highly REE undersaturated granitic melt forcing complex substitutions in accessories to stabilize them. Major minerals (feldspars, garnet, cordierite, biotite) in migmatites from granulite terranes do not show important concentrations of those trace elements but they can locally control the chemistry of the included accessory mineral (e.g. monazite in garnet or cordierite) involving the participation of accessories in major-phase reactions. Thus, there is a redistribution of trace elements (REE, Y, Th, U, P) between accessories and major minerals as well as granitic melts in the early stages of granulite-facies conditions.

This situation changes in lower crustal scenarios where major minerals have very high contents of trace elements thus becoming the main host of the whole-rock (REE–Y–(Zr)) budget. This occurs when Al-Ti-phlogopite is very scarce, close to total mica consumption during granulite-facies metamorphism (last biotite-out isograd). A marked redistribution of HREE–Y–Zr between garnet and xenotime (until its disappearance) and zircon, but also of LREE between feldspars (K-feldspar and plagioclase) and monazite, is suggested. An intimate relationship between major and accessory phases during metamorphic reactions is deduced at high-grade granulite facies conditions as suggested recently by Pyle and Spear (1999). These observations have important implications in application of partitioning-based mineral–mineral and melt–mineral equilibria, which will be explored in future studies.

Acknowledgements

The authors thank the CAI-Microscopía electrónica de la UCM and A. Fernández Larios and J. González Tánago for SEM and electron microprobe facilities. Hilary Downes is warmly thanked for her detailed and constructive comments. Detailed revisions made by J. Pyle, F. Bea and R. Rudnick greatly improved the quality of the work. This work has been supported by the Spanish Interministry Commission for Science and Technology, project BTE2000-0575. **[RR]**

Appendix A. LA-ICP-MS analyses of ATHO-G reference sample

	ATHO-G					
	NIST 612 Calibration (ppm)	Measured (ppm), $n=7$	S.D.	Coefficient variation	Reference (ppm)	(% diff.)
V	43.9	3.0	0.2	6.7	(4.4)	−31.8
Cr	27.0	4.9	1.2	24.5	6	−18.3
Ni	51.4	3.6	0.7	19.4	(17)	−78.8
Rb	34.1	52.9	1.4	2.7	63.8	−17.1
Sr	81.8	79.1	2.4	3.0	96.4	−17.9
Y	39.6	82.8	1.7	2.1	93.8	−11.7
Zr	35.5	606.3	14.6	2.4	524	+15.7
Ba	41.0	476.7	17.2	3.6	553	−13.8
La	38.6	50.7	1.2	2.4	55.5	−8.6
Ce	42.3	111.5	3.1	2.8	124	−10.1
Nd	39.8	55.7	1.9	3.4	61.3	−9.2
Sm	37.9	13.2	0.8	6.1	14.6	−9.4
Eu	37.4	2.5	0.2	8.0	2.84	−12.2
Gd	41.3	13.5	0.8	5.9	15.5	−13.1
Dy	39.8	15.1	1.1	7.3	15.6	−3.5
Yb	42.0	10.6	0.7	6.6	10.1	+4.9
Lu	40.6	1.5	0.1	6.7	1.52	−3.5
Hf	38.4	12.2	0.8	6.6	13.6	−10.1
Pb	40.3	6.4	0.5	7.8	5.7	+11.8
Th	39.4	8.8	0.6	6.8	7.48	+17.6
U	39.0	2.5	0.3	12.0	2.35	+5.0

Reference concentration values for ATHO-G (Iceland rhyolite glass) are from Jochum et al. (2000) except ( ) which are only information values (Jochum et al., 2000).

(% diff.) is the percent deviation between measured and expected values.

Appendix B. Granulite bulk rock geochemistry

	Sotosalbos Complex						Toledo Complex					Xenoliths	
	Av. orthogneiss	100563 Sotosalbos granite	102181 N-leucosome	102183 Leucogranite	101637[a] Melanosome	100562[a] Bt-rich enclave	89103[b] Layos granite	93201[b] N-Leucosome	93197[b] E-Leucosome	81925 Cervatos leucogranite	93198[b] Melanosome	77750[c] Pelitic xenolith	99185 Felsic xenolith
SiO_2	66.15	68.62	74.43	71.81	60.96	43.19	61.37	68.92	69.50	73.49	57.15	55.02	64.80
TiO_2	0.61	0.51	0.03	0.14	0.8	1.81	0.61	0.13	0.52	0.04	1.13	1.28	1.86
Al_2O_3	16.47	15.78	13.95	15.32	18.53	27.65	18.45	16.91	14.96	14.40	20.16	24.72	14.95
Fe_2O_3	5.19	4.11	0.62	1.10	8.12	13.57	7.11	1.56	2.56	1.20	9.39	9.94	8.73
MnO	0.05	0.04	0.01	0.02	0.08	0.07	0.09	0.01	0.01	0.02	0.08	0.06	0.10
MgO	1.67	1.37	0.13	0.23	2.58	3.44	2.68	0.48	0.91	0.36	3.39	2.29	3.22
CaO	1.61	1.31	0.59	0.80	1.66	0.65	0.81	1.31	0.86	1.20	1.54	0.41	1.40
Na_2O	2.88	2.95	2.45	3.14	2.34	1.38	2.01	2.75	1.83	3.23	1.79	0.63	1.87
K_2O	3.68	3.88	6.92	6.51	3.1	6.54	4.05	6.5	7.00	4.56	3.90	3.42	2.27
P_2O_5	0.30	0.26	0.16	0.13	0.5	0.1	0.23	0.3	0.34	0.21	0.13	0.13	0.13
LOI	1.35	1.11	0.56	0.56	1.58	1.56	2.20	0.76	1.16	1.04	1.06	1.76	0.78
Total	99.94	99.94	99.85	9.76	100.25	99.96	99.00	99.62	99.64	99.75	99.72	99.66	100.11
Ba	969	613	858	828	191	536	604	1341	1174	714	762	929	906
Rb	153	177	197	211	279	501	161	236	220	81	175	108	56
Sr	173	148	137	213	88	79	173	276	247	182	237	141	248
Y	47.10	33.10	7.12	41.00	66	24	23	11	8	4.15	27	46	52.6
Zr	269	186	17	39	296	406	123	48	166	55	218	247	2018
Nb	10.17	10.21	1.58	4.35	16	39	13	5	9	0.83	21	21	26.9
Th	20.14	12.23	1.47	5.18	25	19	16	5	22	2.71	19	22	2.42
U	4.33	7.10	1.11	5.57	5	6	5	nd	nd	1.07	nd	nd	1.09
V	69	59	6	5	107	268	111	14	37	5	139	156	172
Cr	290	256	76	20	607	249	364	6	25	164	145	246	119
Ni	33	26	3	3	51	99	65	5	10	13	57	36	29
La	51.86	28.43	3.67	13.10	53.7	60.51	33.55	23.15	50.98	8.59	69.41	68.14	35.50
Ce	105.55	59.27	7.11	26.90	113.03	129.81	64.50	43.79	114.57	16.30	135.75	130.90	61.50
Nd	46.09	29.50	3.24	11.10	58.4	65.45	29.13	21.5	51.31	6.38	54.80	63.95	23.50
Sm	10.13	5.88	0.81	2.88	13.18	12.87	6.53	5.34	11.87	1.06	11.05	11.80	5.65
Eu	1.67	1.22	1.13	1.62	0.85	1.21	1.25	2.21	2.06	1.10	1.93	2.24	1.96
Gd	8.35	4.97	0.92	3.56	12.12	8.63	5.43	4.62	9.65	0.81	9.03	9.05	8.33
Dy	7.64	5.14	1.02	5.00	11.86	5.28	4.54	3.36	3.95	0.69	7.07	7.59	7.88
Er	4.67	2.94	0.61	3.44	5.48	2.27	3.05	1.5	1.14	0.46	3.70	4.45	5.32
Yb	4.88	2.96	0.61	3.85	5.47	2.1	4.25	1.27	0.51	0.77	3.30	4.33	4.99
Lu	0.81	0.43	0.09	0.50	0.71	0.35	0.82	0.23	0.13	0.13	0.59	0.60	0.86

[a] Data from Villaseca et al. (2001).
[b] Data from Barbero et al. (1995).
[c] Data from Villaseca et al. (1999).

References

Barbero, L., 1995. Granulite-facies metamorphism in the Anatectic Complex of Toledo, Spain: late Hercynian tectonic evolution by crustal extension. J. Geol. Soc. (Lond.) 152, 365–382.

Barbero, L., Rogers, G., 1999. Implications of U–Pb monazite ages from syn-orogenic granites of the Anatectic Complex of Toledo (Spain) in the evolution of the central part of the Hercynian Iberian Belt. Doc. BRGM 290, 203.

Barbero, L., Villaseca, C., 2000. Eclogite facies relics in metabasites from the Sierra de Guadarrama (Spanish Central System): *P–T* estimations and implications for the Hercynian evolution. Mineral. Mag. 64, 815–836.

Barbero, L., Villaseca, C., Rogers, G., Brown, P.E., 1995. Geochemical and isotopic disequilibrium in crustal melting: an insight from anatectic granitoids from Toledo, Spain. J. Geophys. Res. 100B8, 15745–15765.

Bea, F., 1996. Residence of REE, Y, Th and U in granites and crustal protoliths: implications for the chemistry of crustal melts. J. Petrol. 37, 521–532.

Bea, F., Montero, P., 1999. Behaviour of accessory phases and redistribution of Zr, REE, Y, Th, and U during metamorphism and partial melting of metapelites in the lower crust: an example from the Kinzigite Formation of Ivrea, Verbano, NW Italy. Geochim. Cosmochim. Acta 63, 1133–1153.

Bea, F., Pereira, M.D., Stroh, A., 1994. Mineral/leucosome trace-element partitioning in a peraluminous migmatite (a laser ablation-ICP-MS study). Chem. Geol. 117, 291–312.

Bea, F., Montero, P., Garuti, G., Zacharini, F., 1997. Pressure-dependence of rare earth element distribution in amphibolite- and granulite-grade garnets. Geostand. Newsl. 21, 253–270.

Bea, F., Montero, P., Molina, J.F., 1999. Mafic precursors, peraluminous granitoids, and late lamprophyres in the Avila Batholith: a model for the generation of variscan batholiths in Iberia. J. Geol. 107, 399–419.

Bingen, B., Demaiffe, D., Hertogen, J., 1996. Redistribution of rare earth elements, thorium, and uranium over accessory minerals in the course of amphibolite to granulite facies metamorphism: the role of apatite and monazite in orthogneisses from southwestern Norway. Geochim. Cosmochim. Acta 60, 1341–1354.

Escuder Viruete, J., Hernáiz, P.P., Valverde-Vaquero, P., Rodriguez, R., Dunning, G., 1998. Variscan syncollisional extension in the Iberian Massif: structural, metamorphic and geochronological evidence from the Somosierra sector of the Sierra de Guadarrama (Central Iberian Zone, Spain). Tectonophysics 290, 87–109.

Franz, G., Andrehs, G., Rhede, D., 1996. Crystal chemistry of monazite and xenotime from Saxothuringian–Moldanubian metapelites, NE Bavaria, Germany. Eur. J. Mineral. 8, 109–118.

Fraser, G., Ellis, D., Eggins, S., 1997. Zirconium abundance in granulite-facies minerals, with implications for zircon geochronology in high-grade rocks. Geology 25, 607–610.

Gerdes, A., Wörner, G., Henk, A., 2000. Post-collisional granite generation and HT–LP metamorphism by radiogenic heating: the Variscan South Bohemian Batholith. J. Soc. Lond. 157, 577–587.

Gromet, L.P., Silver, L.T., 1983. Rare earth element distribution among minerals in a granodiorite and their petrogenetic implications. Geochim. Cosmochim. Acta 47, 925–939.

Hanchar, J.M., Rudnick, R.L., 1995. Revealing hidden structures: the application of cathodoluminescence and back-scattered electron imaging to dating zircons from lower-crustal xenoliths. Lithos 36, 289–303.

Harris, N.B.W., Gravestock, P., Inger, S., 1992. Ion-microprobe determinations of trace-element concentrations in garnets from anatectic assemblages. Chem. Geol. 100, 41–49.

Heinrich, W., Andrhes, G., Franz, G., 1997. Monazite–xenotime miscibility gap thermometry: I. An empirical calibration. J. Metamorph. Geol. 15, 3–16.

Hoskin, P.W.O., Ireland, T.R., 2000. Rare element chemistry of zircon and its use as a provenance indicator. Geology 28, 627–630.

Hoskin, P.W.O., Kinny, P.D., Wyborn, D., Chappell, B.W., 2000. Identifying accessory mineral saturation during differentiation in granitoid magmas: an integrated approach. J. Petrol. 41, 1365–1396.

Jarosewich, E.J., Boatner, L.A., 1991. Rare-earth element reference samples for electron microprobe analysis. Geostand. Newsl. 15, 397–399.

Jochum, K.P., Dingwell, D.B., Rocholl, A., Stoll, B., Hofman, A.W., Becker, S., Beshmen, A., Bessette, D., Dietze, H.J., Dulski, P., Erzinger, J., Hellebrand, E., Hoppe, P., Horn, I., Janssens, K., Jenner, G.A., Klein, M., McDonough, W.F., Maetz, M., Mezger, K., Münker, C., Nikogosian, I.K., Pickhardt, C., Raczek, I., Rhede, D., Seufert, H.M., Simakin, S.G., Sobolev, A.V., Spettel, B., Straub, S., Vincze, L., Wallianos, A., Weckwerth, G., Weyer, S., Wolf, D., Zimmer, M., 2000. The preparation and preliminary characterisation of eight geological MPI-DING reference glasses for in-situ microanalysis. Geostand. Newsl. 24, 87–133.

Johannes, W., Holtz, F., Möller, P., 1995. REE distribution in some layered migmatites: constraints on their petrogenesis. Lithos 35, 139–152.

Kretz, R., 1983. Symbols for rock forming minerals. Am. Mineral. 68, 277–279.

Kretz, R., Campbell, J.L., Hoffman, E.L., Hartree, R., Teesdale, J., 1999. Approaches to equilibrium in the distribution of trace elements among the principal minerals in a high-grade metamorphic terrane. J. Metamorph. Geol. 17, 41–59.

Longeritch, H.P., Jackson, S.E., Günter, D., 1996. Laser ablation inductively coupled plasma mass spectrometric transient signal data acquisition and analyte concentration calculation. J. Anal. At. Spectrom. 11, 899–904.

Loock, G., Stosch, H.G., Seck, H.A., 1990. Granulite facies lower crustal xenoliths from the Eifel, West Germany: petrological and geochemical aspects. Contrib. Mineral. Petrol. 105, 25–41.

Martín Romera, C., Villaseca, C., Barbero, L., 1999. Materiales anatécticos en el área de Sotosalbos (Segovia, Sierra de Guadarrama). Caracterización petrológica, geoquímica e isotópica (Sr, Nd). Actas II Congr. Ibérico Geoquim., Lisb., 329–332.

Montel, J.M., 1993. A model for monazite/melt equilibrium and application to the generation of granitic magmas. Chem. Geol. 110, 127–146.

Nabeleck, P.I., Glascock, D., 1995. REE-depleted leucogranites,

Black Hills, south Dakota: a consequence of disequilibrium melting of monazite-bearing schists. J. Petrol. 36, 1055–1071.

Nash, W.P., Crecraft, H.R., 1985. Partition coefficients for trace element in silicic magmas. Geochim. Cosmochim. Acta 49, 2309–2322.

Nemchin, A.A., Giannini, L.M., Bodorkos, S., Oliver, N.H.S., 2001. Ostwald ripening as a possible mechanism for zircon overgrowths formation during anatexis: theoretical constraints, a numerical model, and its application to pelitic migmatites of the Tickalara Metamorphics, northwestern Australia. Geochim. Cosmochim. Acta 65, 2771–2788.

Otamendi, J.E., de la Rosa, J.D., Patiño Douce, A.E., Castro, A., 2002. Rayleigh fractionation of heavy rare earths and yttrium during metamorphic garnet growth. Geology 30, 159–162.

Pan, Y., 1997. Zircon- and monazite-forming metamorphic reactions at Manitouwadge, Ontario. Can. Mineral. 35, 105–118.

Pan, Y., Fleet, M.E., Longstaffe, F.J., 1999. Melt-related metasomatism in mafic granulites of the Quetico subprovince, Ontario: constraints from O–Sr–Nd isotopic and fluid inclusion data. Can. J. Earth Sci. 36, 1449–1462.

Pereira, M.D., Rodriguez Alonso, M.D., 2000. Duality of cordierite granites related to melt-restite segregation in the Peña Negra anatectic complex, central Spain. Can. Mineral. 38, 1329–1346.

Pride, C., Muecke, G.K., 1981. Rare earth element distributions among coexisting granulite facies minerals, Scourian Complex, NW Scotland. Contrib. Mineral. Petrol. 76, 463–471.

Pyle, J.M., Spear, F.S., 1999. Yttrium zoning in garnet: coupling of major and accessory phases during metamorphic reactions. Geol. Mater. Res. 1, 1–49.

Pyle, J.M., Spear, F.S., Rudnick, R.A., McDonough, W.F., 2001. Monazite–Xenotime–Garnet equilibrium in metapelites and a new monazite–garnet thermometer. J. Petrol. 42, 2083–2107.

Reid, M.R., 1990. Ionprobe investigation of rare earth element distribution and partial melting of metasedimentary granulites. In: Vielzeuf, D., Vidal, Ph. (Eds.), Granulites and Crustal Evolution. Kluwer Academic Publishing, Dordrecht (The Netherlands), pp. 507–522.

Rubbatto, D., 2002. Zircon trace element geochemistry: partitioning with garnet and the link between U–Pb ages and metamorphism. Chem. Geol. 184, 123–138.

Rubbatto, D., Williams, I.S., Buick, I.S., 2001. Zircon and monazite response to prograde metamorphism in the Reynolds Range, central Australia. Contrib. Mineral. Petrol. 140, 458–468.

Schaltegger, U., Fanning, C.M., Günther, D., Maurin, J.C., Schulmann, K., Gebauer, D., 1999. Growth, annealing and recrystallization of zircon and preservation of monazite in high-grade metamorphism: conventional and in-situ U–Pb isotope, cathodoluminiscence and microchemical evidence. Contrib. Mineral. Petrol. 134, 186–201.

Schwandt, C.S., Papike, J.J., Shearer, C.K., 1996. Trace element zoning in pelitic garnet of the Black Hills, South Dakota. Am. Mineral. 81, 1195–1207.

Solar, G.S., Brown, M., 2001. Petrogenesis of migmatites in Maine, USA: possible source of peraluminous leucogranite in plutons? J. Petrol. 42, 789–823.

Spear, F.K., Kohn, M.J., 1996. Trace element zoning in garnet as a monitor of crustal melting. Geology 24, 1099–1102.

Tanner, D.C., Behrmann, J.A., 1997. Study of strain and partial-melt transfer in a banded migmatite. J. Struct. Geol. 19, 1405–1417.

Villaseca, C., Herreros, V., 2000. A sustained felsic magmatic system: the Hercynian granitic batholith of the Spanish Central System. Trans. R. Soc. Edinb. Earth Sci. 91, 207–219.

Villaseca, C., Barbero, L., Rogers, G., 1998. Crustal origin of Hercynian peraluminous granitic batholiths of central Spain: petrological, geochemical and isotopic (Sr, Nd) constraints. Lithos 43, 55–79.

Villaseca, C., Downes, H., Pin, C., Barbero, L., 1999. Nature and composition of the lower continental crust in central Spain and the granulite–granite linkage: inferences from granulitic xenoliths. J. Petrol. 40, 1465–1496.

Villaseca, C., Martín Romera, C., Barbero, L., 2001. Melts and residua geochemistry in a low-to-mid crustal section (Central Spain). Phys. Chem. Earth 26, 273–280.

Wark, D.A., Miller, C.F., 1993. Accessory mineral behavior during differentiation of a granite suite: monazite, xenotime and zircon in the Sweetwater Wash pluton, southeastern California, USA. Chem. Geol. 110, 49–67.

Watson, E.B., 1996. Dissolution, growth and survival of zircons during crustal fusion: kinetic principles, geological models and implications for isotopic inheritance. Trans. R. Soc. Edinb. Earth Sci. 87, 43–56.

Watt, G.R., Harley, S.L., 1993. Accessory phase controls on the geochemistry of crustal melts and restites produced during water-undersaturated partial melting. Contrib. Mineral. Petrol. 114, 550–566.

Watt, G.R., Burns, I.M., Graham, G.A., 1996. Chemical characteristics of migmatites: accessory phase distribution and evidence for fast melt segregation rates. Contrib. Mineral. Petrol. 125, 100–111.

Wolf, M.B., London, D., 1995. Incongruent dissolution of REE- and Sr-rich apatite in peraluminous granitic liquids: differential apatite, monazite, and xenotime solubilities during anatexis. Am. Mineral. 80, 765–775.

Yurimoto, H., Duke, E.F., Papike, J.J., Shearer, C.K., 1990. Are discontinuous chondrite-normalized REE patterns in pegmatite granite systems the result on monazite fractionation? Geochim. Cosmochim. Acta 54, 2141–2145.

Zhu, X.K., O'Nions, R.K., 1999. Zonation of monazite in metamorphic rocks and its implications for high temperature thermochronology: a case study from the Lewisian terrain. Earth Planet. Sci. Lett. 171, 209–220.